JGR Oceans

RESEARCH ARTICLE
10.1029/2021JC017169

Special Section:
Southern Ocean and Climate: Biogeochemical and Physical Fluxes and Processes

Key Points:

- Data from Biogeochemical-Argo floats reveal nitrate injections that last up to 3.5 months at 300 m depth and span distances up to 295 km
- The nitrate injections reach 100 m depth and are often followed by an increase in satellite observed chlorophyll
- The injections develop within cyclonic eddies, usually during a change in eddy dynamics, and often near a frontal zone between eddies

Supporting Information:

Supporting Information may be found in the online version of this article.

Correspondence to:
C. Wilson,
cara.wilson@noaa.gov

Citation:
Wilson, C. (2021). Evidence of episodic nitrate injections in the oligotrophic North Pacific associated with surface chlorophyll blooms. *Journal of Geophysical Research: Oceans*, *126*, e2021JC017169. https://doi.org/10.1029/2021JC017169

Received 6 JAN 2021
Accepted 9 OCT 2021

Evidence of Episodic Nitrate Injections in the Oligotrophic North Pacific Associated With Surface Chlorophyll Blooms

Cara Wilson[1]

[1]Environmental Research Division, Southwest Fisheries Science Center, National Marine Fisheries Service, National Oceanic and Atmospheric Administration, Monterey, CA, USA

Abstract Summer blooms of chlorophyll develop in the oligotrophic North Pacific Ocean between Hawaii and 30°N. It is thought that episodic injections of subsurface nutrients fuel these blooms, but the exact mechanism is unknown. Here data from Biogeochemical-Argo floats are examined to look for evidence of subsurface mixing that could stimulate these surface chlorophyll features. Data are examined from 25 floats that measured 5,569 profiles near Hawaii between September 2002 to April 2021. Since not all floats had nitrate sensors, but all floats had oxygen sensors, nitrate concentrations were calculated from oxygen measurements using the "CArbonate system and Nutrients concentration from hYdrological properties and Oxygen using a Neural-network" model. There were 14 times when the nitracline, defined as the depth where nitrate is 1 μmol kg^{-1}, reached 100 m during the summer (June–September). In six of these 14 episodes, the nitracline anomaly was the result of shoaling isopycnals. During the other eight episodes nitrate increased along isopycnal surfaces, indicating diapycnal mixing was occurring. In these events, referred to as injection events, perturbations to the vertical nitrate distribution extended all the way down to 300 m depth, and lasted up to 3.5 months, spanning hundreds of kilometer. Seven of the eight injection events occurred within cyclonic eddies, one occurred within an anticyclonic eddy. The timing of the injection events often coincided with a change in eddy dynamics, either eddy speed or eddy transformation. The injection events in cyclonic eddies were followed by a surface increase in chlorophyll in the surrounding area as observed in satellite data.

Plain Language Summary Satellite data have revealed large expanses of increased phytoplankton in the North Pacific Ocean, that develop during summer between Hawaii and California. These blooms are probably fueled by subsurface nutrient injections, but the exact mechanism is not known. To understand this phenomenon requires nutrient data in the surface water during their development. But such data are difficult to acquire with traditional ship surveys because of the large area where the blooms develop. However, there are ocean floats that acquire profiles of physical and chemical data every few days, and some of these have been deployed in the bloom region. Here these float data are examined and they show episodes when deep, nutrient-rich water rises up into the surface water. When these events occur in summer, they are followed by the development of a chlorophyll bloom as seen in satellite data. Seven of the eight injection events occurred within cyclonic eddies, one occurred within an anticyclonic eddy. The timing of the injection events often coincided with a change in eddy dynamics, either eddy speed or eddy transformation. This is the first time we have subsurface biogeochemical data concurrent with the development of a chlorophyll bloom in this region.

1. Introduction

Satellite ocean color data have revealed large chlorophyll blooms in the North Pacific Subtropical Gyre (NPSG) that cover thousands of km^2 and persist for weeks or longer (Dore et al., 2008; Landry, 2002; White et al., 2007; Wilson & Qiu, 2008). The most intense and most frequent blooms occur between 130–150°W and 28–32°N, but chlorophyll-*a* (chl) blooms also develop further south, in the region just north of Hawaii. The blooms are often made up of diatom-diazotroph assemblages (DDAs) of the diatoms *Hemiaulus* and *Rhizosolenia* containing the nitrogen fixing endosymbiont *Richelia intracellularis* (Anderson et al., 2018; Villareal et al., 2011, 2012). Episodic pulses of these DDAs can rapidly sink and could be responsible for the

summer export pulse in particulate matter export to the deep sea that occurs every mid-July to mid-August in this region (Karl et al., 2012).

The physical dynamics that stimulate the blooms remain unknown. Episodic injections of subsurface nutrients from eddy dynamics are likely the cause but the exact mechanism is unknown. There are two primary ways that eddies can perturb the vertical distribution of nutrients. Upwelling in the center of cyclonic eddies can lift up isopycnals and isopleths of nutrients into the euphotic zone, a process termed eddy pumping (Falkowski et al., 1991; Martin & Pondaven, 2003; McGillicuddy & Robinson, 1997). Cyclonic eddies exhibiting eddy pumping behavior regularly occur in the lee of Hawaii (Benitez-Nelson & McGillicuddy, 2008; Nencioli et al., 2008; Seki et al., 2001).

Another mechanism is submesoscale frontal processes that occur at the periphery of eddies, and can induce large vertical velocities (Lévy, 2008; Mahadevan et al., 2008; Spall & Richards, 2000). A number of authors have evoked this mechanism, vertical velocities driven by frontogenesis, to explain the NPSG chl blooms (Calil et al., 2011; Calil & Richards, 2010; Guidi et al., 2012). However, Ascani et al. (2013) argued this process would not be effective in the NPSG, where there is a large vertical offset between the frontal processes in the surface layer and the deep nitracline (at ∼150 m depth). However, the eddy field clearly plays a role in the dynamics of the surface chl blooms since they are usually wrapped around eddies, in a manner consistent with horizontal stirring concentrating chl in convergence zones (Calil et al., 2011; Calil & Richards, 2010; Guidi et al., 2012). Associated with horizontal stirring, dilution and dispersal effects can reduce the amount of grazing, which will also help to sustain the blooms (Lehahn et al., 2017). The chl blooms generally develop near 30°N (Wilson & Qiu, 2008), a latitude that has been called a critical latitude (Dong et al., 2019; Hibiya et al., 2007; MacKinnon & Winters, 2005) because dynamics occur there which can lead to enhanced mixing. It has also been proposed that the blooms could be stimulated by nutrient injection from breaking internal waves at the critical latitude (Wilson, 2011).

The proposed mechanisms of nutrient injection are impossible to investigate without in situ data, which are difficult to obtain in this relatively isolated part of the ocean. There have been a number of cruises in this area at the time of year when the blooms develop (Guidi et al., 2012; Shcherbina et al., 2010; Villareal et al., 2011, 2012; Wilson et al., 2013), but the limited temporal and spatial resolution that can be obtained with shipboard observations makes these measurements ill-suited to capture episodic phenomena in the ocean. Monthly measurements of physical and biogeochemical parameters have been made at the Hawaii Ocean Time-series (HOT) station at 22°45'N, 158°W since 1998 (Karl & Lukas, 1996), and episodic injections of nitrate into the euphotic zone are evident in the HOT data, appearing almost every year (Karl et al., 2008). However, it is likely that the monthly sampling of the HOT program could miss short-lived events occurring between measurements. Additionally, given the spatial variability in the surface chl distribution in this region (Wilson & Qiu, 2008), data are needed that have more spatial coverage than can be obtained from eularian measurements.

There have been 32 Biogeochemical-Argo (BGC-Argo) floats (Claustre et al., 2020) deployed around Hawaii in the North Pacific. Data from some of these floats have been used to examine biochemical processes in this region, including observations of episodic subsurface injections of nitrate (Ascani et al., 2013; Johnson et al., 2010; Riser & Johnson, 2008; Xiu & Chai, 2020). Johnson et al. (2010) concluded that subsurface nitrate injection is a major factor sustaining productivity in the NPSG, but they also noted that this transport of nitrate is not sufficient to support the amount of production occurring in the mixed layer, and suggested that biologically induced transport by vertically migrating phytoplankton (Villareal et al., 1999, 2014) could be a factor. Ascani et al. (2013) concluded that the observed nitrate anomalies are largely associated with vertical displacements of isopycnal surfaces from changes in the eddy field. Xiu and Chai (2020) observed that uplift of the nitracline in cyclonic eddies enhanced chl in the subsurface chl maximum. Evidence of late summer blooms was also inferred from excess oxygen production within the subsurface oxygen maximum (Riser & Johnson, 2008). These previous studies of BGC-Argo data in the NPSG have focused on the subsurface dynamics, but none of them have looked at the possible connection between subsurface dynamics and the surface chl blooms observed by satellite data. There have been some studies that have examined BGC-Argo data in conjunction with satellite chl blooms in other regions (Jayaram et al., 2019; Lotliker et al., 2018; Mayot et al., 2017; Sauzède et al., 2020).

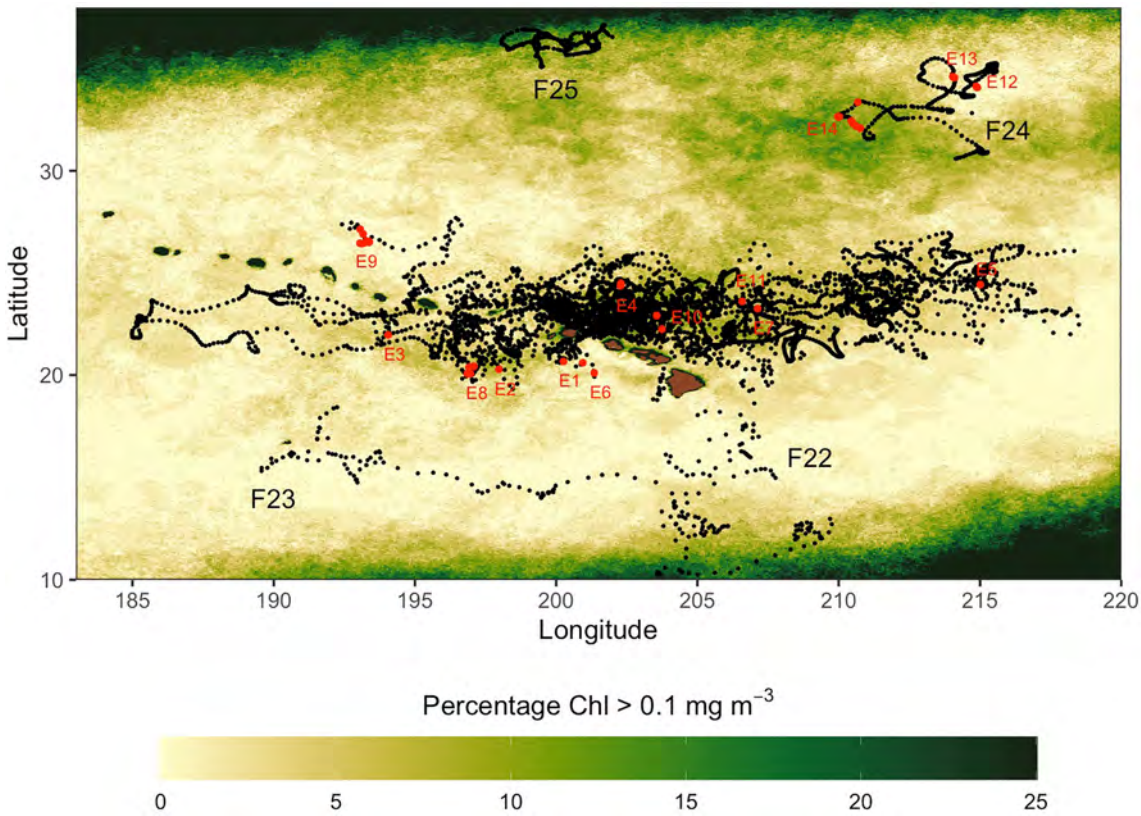

Figure 1. Map of profile locations from 25 float profiles in the North Pacific Subtropical Gyre. Red points indicate profiles with nitrate >1 μmol kg^{-1} at 100 m in the summer (June–September). Overlain is the percentage of times satellite chl > 0.1 mg/m^3 in July–October of 1997–2020 from weekly OC-CCI data, indicating the locations where chl blooms develop the most frequently.

Here the BGC-Argo float data from the NPSG (between 10°40°N, and 140°–180°W) are analyzed to look for evidence of subsurface injections that could be driving the chl blooms observed in satellite data. Since 2002, 32 BGC-Argo floats have been deployed in this region. Here data from 25 of these floats are examined (Figure 1). This data set comprises 5,569 profiles between 177°–141°W and 10°–37°N, and is substantially larger than has previously been examined for evidence of subsurface nutrient injections (Ascani et al., 2013; Johnson et al., 2010). Since not all floats had nitrate sensors, but all floats had oxygen sensors, nitrate concentrations were calculated from oxygen measurements using the CArbonate system and Nutrients concentration from hYdrological properties and Oxygen using a Neural-network (CANYON-B) model (Bittig et al., 2018; Sauzède et al., 2017). Satellite chl data from the Ocean Colour Climate Change Initiative (OC-CCI) data set (Sathyendranath et al., 2019) are used to examine the surface conditions around several large subsurface injection events. Sea-level anomalies (SLA) derived from satellite altimetry and eddy trajectory data (Chelton et al., 2011; Schlax & Chelton, 2016) are used to look at the relationship between subsurface injections, eddy dynamics and the development of surface chl blooms.

2. Data

2.1. BGC-Argo Floats

The synthetic profile data files (Bittig et al., 2021) from 32 BGC-Argo floats in the NPSG region (Figure 1) were downloaded from https://biogeochemical-argo.org/data-access.php. The data have undergone quality control checking and adjustments for initial sensor calibration errors by the Argo data management team (Bittig et al., 2019; Schmechtig et al., 2015; Thierry et al., 2021), and the adjusted values were used for all parameters. The parameters measured by the floats vary (Table 1), however all floats measured temperature, salinity, and oxygen. The floats were all Autonomous Profiling Explorers (APEX) with optode

Table 1
List of Information on the 25 BGC-Argo Floats Used Here

Float ID	WMO ID	Average Lat (°N)	Average Long (°W)	Start	End	N	Average Δtime (days)	Duration (years)	Parameters	Events
F1	4900093	23.2	155.2	09/08/02	06/27/05	96	10.8	2.81		
F2	5900952	21.6	160.9	06/03/05	03/18/07	118	5.6	1.79		E1, E2
F3	5901069	25.4	164.1	03/13/06	08/11/07	101	5.2	1.42		E9
F4	5901071	23.0	158.8	05/29/06	03/12/09	203	5.0	2.80		
F5	5901073	22.5	156.7	05/29/06	02/11/08	122	5.1	1.71		
F6	5901072	22.2	148.8	08/20/06	05/11/12	213	9.9	5.74		
F7	5901468	23.4	151.4	12/23/07	10/22/11	239	5.9	3.84	N	
F8	1901379	23.1	162.9	11/06/09	11/05/13	293	5.0	4.01	N	E3
F9	5903272	23.4	157.4	05/21/10	06/25/15	360	5.2	5.11	N	E4
F10	5903611	22.8	164.7	11/03/11	11/09/17	299	5.2	6.04	N	
F11	5903385	23.8	152.5	01/10/11	04/08/15	426	5.2	4.26	N	E3
F12	5903741	24.1	151.0	03/27/12	02/20/21	260	12.6	8.93	P	E5
F13	5903888	24.3	151.2	07/09/12	01/07/18	279	7.2	5.52		
F14	5903893	23.0	150.6	10/03/12	05/05/16	264	5.0	3.60	P	E7
F15	5904093	21.7	162.1	02/15/13	10/29/18	272	7.7	5.72		E6, E8
F16	5904094	22.4	157.7	02/15/13	01/04/17	285	5.0	3.90	N	E11
F17	5904124	24.7	150.3	05/20/13	06/02/16	221	5.0	3.05	N, C, B, P	
F18	5904172	22.5	157.9	01/18/14	09/15/14	65	3.8	0.66	N, C, B, P	
F19	5906040	23.5	157.0	06/14/19	04/04/21	242	2.7	1.81	N, C, B, P	E10
F20	5906039	22.1	153.7	07/04/19	06/04/20	299	1.1	0.92	N, C, B, P	
F21	5901336	23.1	157.4	08/21/06	12/14/10	156	10.2	4.33		
F22	5901337	15.5	154.2	08/21/06	07/14/07	37	9.1	0.90		
F23	5901339	13.9	159.3	08/22/06	05/07/11	170	10.2	4.72		
F24	5904128	33.4	146.3	07/31/13	07/18/17	280	5.2	3.98	N	E12, E13, E14
F25	5904127	36.3	159.9	07/07/13	05/02/17	269	5.2	3.83	N	

Note. The abbreviated float number used here is shown along with the WMO float ID, the average latitude, average longitude, the start and end dates, the number of profiles, the average number of days between profiles, and which parameters other than oxygen were measured. N = nitrate, C = chl, B = backscatter and P = pH. The injection events observed by the floats are also indicated. BGC-Argo, Biogeochemical-Argo.

oxygen sensors. Oxygen data from the BGC-Argo floats has been found to be accurate to within 1% (Johnson et al., 2017). All of the oxygen data used had a quality control (QC) flag of 1, indicating that all of the QC tests had been passed (Bittig et al., 2019). Almost all of the data had gone through delayed mode processing. The exception was the most recent data (data collected after August 30, 2020, <1% of the profiles) which were real time data that had been adjusted.

The CANYON-B model (Bittig et al., 2018; Sauzède et al., 2017) was used to calculate nitrate from the float's temperature, salinity, oxygen, and geolocation data. Seven floats were of short duration or had issues with their oxygen sensor and their data were not further analyzed (WMO floats 5900588, 5900958, 5901338, 5903753, 5903754, 5904132, and 5904655). Complete sections of the surface nitrate (top 300 m) from all of the floats are shown in Figure S2 in Supporting Information S1).

Data from 25 floats, named F1-F25 here, were analyzed, spanning a timeframe from September 2002 to April 2021 (Table 1). In total 5,569 float profiles were analyzed. The float trajectories range between 175°–141°W and 10°–37°N (Figure 1), but 85% of the profiles occurred within the narrower latitude range of 20°–26°N (Figure 2). Floats profiled at either 1-, 5- or 10-day intervals (Table 1). Nitrate data from F7–F10

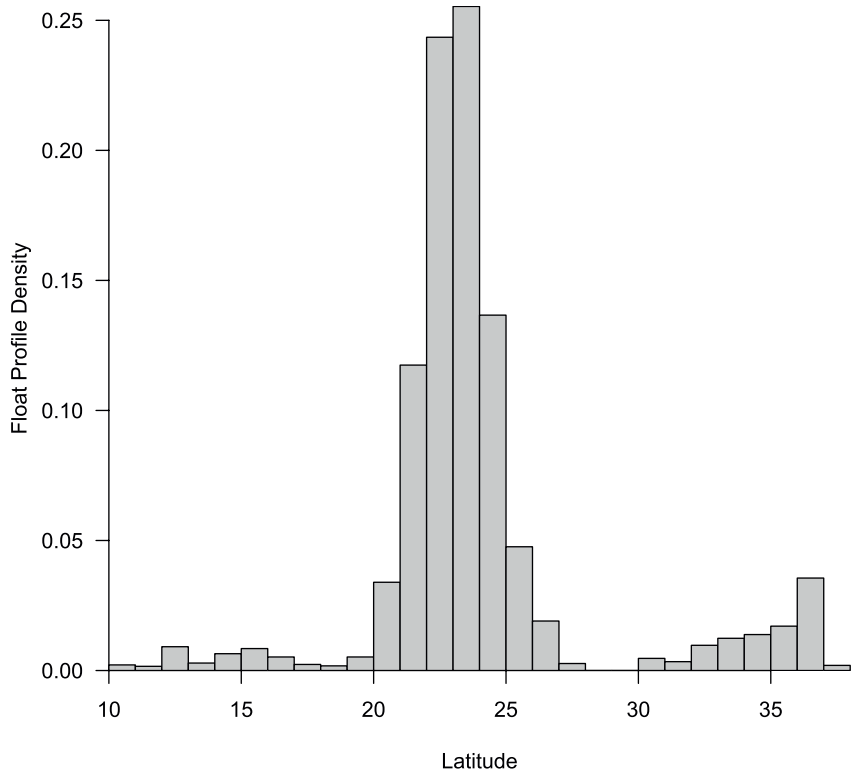

Figure 2. Histogram of the latitude of all 5,569 float profiles. 85% of them occurred between 20–26°N.

and F12 have been published previously (Ascani et al., 2013; Johnson et al., 2010; Xiu & Chai, 2020). Measurements were made every 5 m in the surface 100 m, every 10 m between 100–400 m depth, and every 50 m below 400 m depth (Johnson et al., 2017). Only the top 300 m of data are shown here.

Nitrate anomalies are identified at two depth levels. At 100 m, levels above 1 μmol kg^{-1} are considered anomalous, and at 300 m, levels above 15 μmol kg^{-1} are considered anomalous. Events are identified anomalous nitrate values at 100 m. Because the objective is to look at the connection between nitrate injections and the summer chl blooms, only injections that occurred in June–September are examined. The nitracline depth is calculated as the depth where nitrate is 1.0 μmol kg^{-1} (Ward et al., 1989). The mixed-layer depth (MLD) is calculated as the depth where temperature values are within 0.8°C of the shallowest value (Kara et al., 2003). The MLD varies between 12 and 120 m, with an average value of 67 m across all floats.

2.2. Satellite Data

Weekly composites of chl from the ocean color climate change initiative (OC-CCI) data set (Sathyendranath et al., 2019) at 4 km spatial resolution, were used to look at surface chl values around the injection events. These data were also used to calculate the prevalence of blooms in the region around the float locations (Figure 1). The OC-CCI data set merges data from the SeaWiFS, Aqua-MODIS, MERIS, and VIIRS sensors to create a continuous data product from 1997. The chl satellite data were accessed from the ERDDAP (Simons, 2020) at NOAA's Southwest Fisheries Science Center Environmental Research Division (https://coastwatch.pfeg.noaa.gov/erddap/). Daily Sea Level Anomaly (SLA) data were obtained from the Copernicus Climate Change and Atmosphere Monitoring Services (https://cds.climate.copernicus.eu/).

2.3. Eddy Data

Eddy trajectory and statistics data (version DT2.0exp) were obtained from AVISO+ (https://www.aviso.altimetry.fr). This data set is produced by SSALTO/DUACS, and developed and validated in collaboration with D. Chelton and M. Schlax at the Oregon State University using a modified method (Schlax & Chelton, 2016)

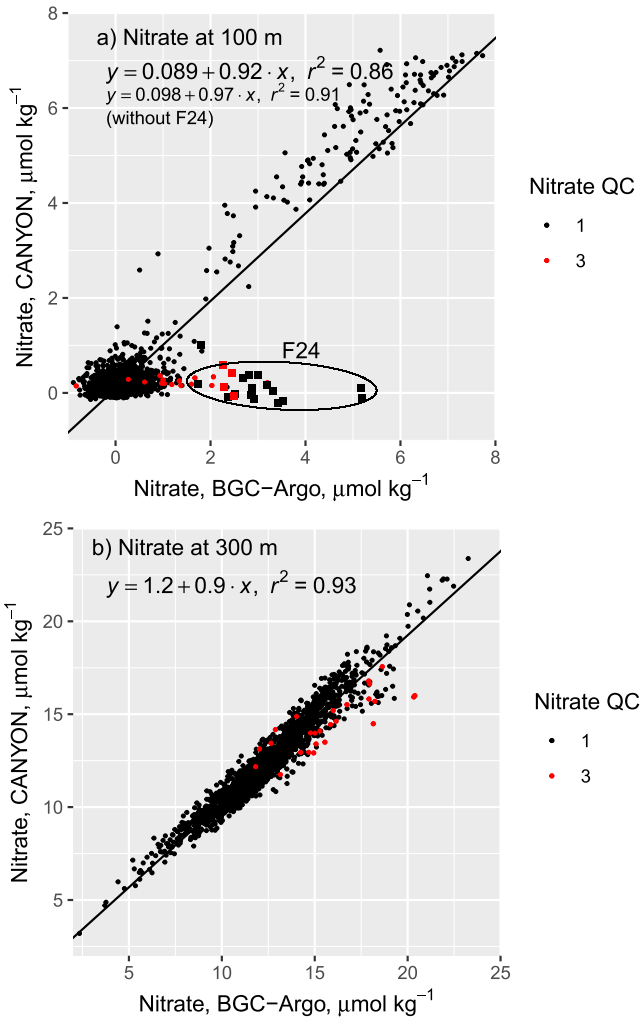

Figure 3. Comparison between nitrate measured by the Biogeochemical-Argo nitrate sensor and nitrate estimated using the "CArbonate system and Nutrients concentration from hYdrological properties and Oxygen using a Neural-network" model from data at (a) 100 m and (b) 300 m depth. Nitrate data measured from the floats with questionable data (QC = 3) are colored red. Data from F24 are shown as squares.

of Chelton et al. (2011). Satellite sea surface height data is used to identify eddies and classify them as either cyclonic or anticyclonic. All eddies are given a unique 6-digit track number, and the rotational speed, amplitude and radius of each eddy are calculated for every point along its trajectory. The proximity to an eddy was determined for each float profile by identifying the closest eddy that was within 0.5° of latitude and longitude (Chelton et al., 2011; Schlax & Chelton, 2016).

3. Results and Discussion

Since not all floats measured nitrate, but all measured oxygen, nitrate was calculated for all floats using the CANYON-B model (Bittig et al., 2018; Sauzède et al., 2017) and temperature, salinity, oxygen, and geolocation data from the float data. Twelve floats measured nitrate (Table 1), and for those floats the nitrate values calculated from the CANYON-B model were compared to those measured from the nitrate sensors for each float separately (Figure S1 in Supporting Information S1). The correlation coefficients range between 0.995–1.0, indicating the CANYON-B model does an excellent job of estimating nitrate from oxygen concentration and physical parameters. To see how this correlation behaves at 100 and 300 m, depths used here to identify events, data were pooled across floats, and correlations between measured and modeled estimated nitrate were made at 100 and 300 m (Figure 3). The data at 100 m are noisier ($r^2 = 0.86$) than the data at 300 m ($r^2 = 0.93$). While some of the nitrate data measured directly from the floats had a QC label of 3 (red points on Figure 3), indicating they are probably bad data (Bittig et al., 2019), the consistent feature of the biggest outliers is not their QC but their float id, they are all from F24 (squares on Figure 3a). If data from F24 is removed the correlation at 100 m increases to $r^2 = 0.91$.

The nitracline depth ranges between 12 and 232 m depth across the study area (Figure 4a). The nitracline is deepest between 20°–25°N, and becomes shallower both equatorward and poleward. North of 36°N the nitracline is always shallower than 100 m. Float profiles at the southern (F22, F23) and northern (F24, F25) boundaries of the NPSG are highlighted on Figure 4. A slightly different pattern occurs with the density of the nitracline. The nitracline density is lowest at low latitudes, ranging between 22.5–24 kg m^{-3} at 10°S, and increases with increasing latitude, to values >25.5 kg m^{-3} above 35°N (Figure 4b).

To identify subsurface nitrate injection that could be precursors to surface chl blooms, profiles with nitrate >1 µmol kg^{-1} at 100 m depth were identified. This analysis excluded data from F23 and F25, as these floats are at the southern and northern boundaries of the gyre (Figure 1), where the nitracline is almost always above 100 m (Figure 4). Of these 5,130 profiles (excluding F23 and F25), the nitracline shoaled past 100 m depth 471 times (9.2%). The events occurring during the late spring and summer are of primary interest here because they could be linked to the surface chl blooms that develop in this region (Dore et al., 2008; Landry, 2002; White et al., 2007; Wilson & Qiu, 2008). Narrowing this analysis to the months of June–September yielded 36 profiles (0.6%). Accounting for the fact that some of these occurrences are clustered together in time and space (Figure 1), resulted in the identification of 14 different events, referred to here as E1–E14 (Table 2). These events were separated into two groups. One group (E1–E8) contains injection events, where nitrate is elevated along isopycnals for many weeks. These injection events are defined as nitrate >15 µmol kg^{-1} at 300 m. The other group (E9–E14) contains events where the nitrate anomalies are the result of shoaling isopycnals without any diapycnal mixing.

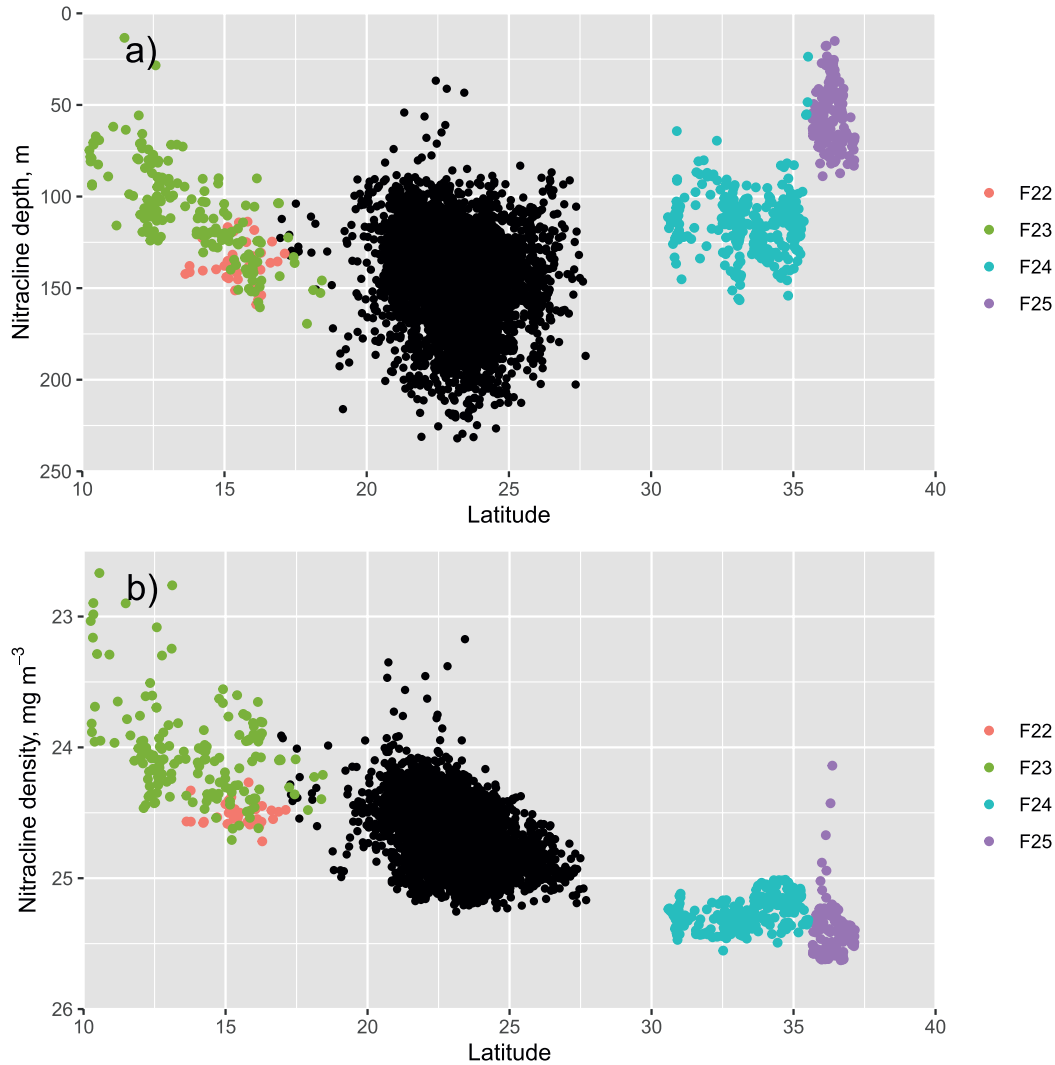

Figure 4. Nitracline (a) depth and (b) density against latitude for all float profiles.

Most of the injection events only had one or two profiles with nitrate >1 μmol kg^{-1} at 100 m depth, suggesting the events are relatively short-lived, however it is evident from the vertical nitrate structure that these events last for several months (Figure 5). Nitrate values above 15 μmol kg^{-1} at 300 m (the yellow lines on Figure 5) are used to identify the duration of these subsurface nitrate injections. The dates and positions of the first and last profiles with nitrate >15 μmol kg^{-1} at 300 m are used to calculate the duration and spatial extent of these events. The summer injections lasted between 10 and 111 days and spanned distances of 30–295 km (Table 2). There is no clear pattern as to when the perturbation at 100 m occurs relative to the start of the event at 300 m. Sometimes the manifestation at 100 m is at the start of the event (E1, E2, E4), sometimes it is in the middle (E3, E5) and sometimes it is at the end (E7). One of the events, E3, was observed at different times and locations by two different floats, F8 and F11 (Figures 5c and 5d). The event observed by F8 occurred in May 2012, about a month before the event in F11, and while there was no signal at 100 m in May in F11 there was at 300 m. The distance between these two floats ranged between 134–202 km during May and June.

The nitrate distribution generally mirrors the density distribution (gray lines on Figure 5), however changes in the iso-nitrate surfaces appear sharper than those of density during the injection events. Nitrate sections plotted against density (Figure 6), confirm that these subsurface injection events cause nitrate anomalies along isopycnal surfaces, indicating diapycnal mixing of nitrate during these events. The iso-nitrate surfaces

Table 2
Summary Information on the 14 Subsurface Injection Events Observed, Including the Date, Latitude, and Longitude of Their Start and Termination, How Long the Events Lasted, the Distance It Spanned, the Track Number for the Eddy or Eddies Associated With the Events, and the Age of the Eddy at the Initiation of the Injection Event

Event	Float	Date, 100 m	Start, 300 m	End, 300 m	Duration at 300 m (days)	Distance at 300 m (km)	Surface Chl increase	Eddy	Eddy age (days)
E1	F2	9/28/2005	9/6/2005	11/7/2005	62	24	Yes	274078	67
E2	F2	7/27/2006	8/13/2006	9/26/2006	44	141	Yes	279677	115
E3	F8	5/10/2012	5/5/2012	5/15/2012	10	47	Yes	321576	56
E3	F11	6/12/2012	5/12/2012	7/8/2012	57	142	Yes	321660	85
E4	F9	7/23/2014	7/23/2014	8/8/2014	16	30	Yes	337839	23
		7/28/2014							
E5	F12	9/9/2014	7/20/2014	10/20/2014	92	76	Yes	335139	210
E6	F15	5/30/2014	5/30/2014	7/8/2014	39	133	Yes	335073	111
		6/22/2014							
		6/30/2014							
E6	F15	8/24/2014	8/16/2014	11/17/2014	93	216	Yes	335073	189
		9/1/2014							
E7	F14	9/26/2014	7/3/2015	10/22/2015	111	295	Yes	344355	37
								342578	127
								345123	-1
E8	F15	7/19/2018	8/28/2018	8/28/2018	< 10	-	No	175009[a]	97
		7/27/2018							
E9	F3	6/25/2007–8/11/2007	-	-	-		No	288000	
E10	F19	9/13/2019	-	-	-		Yes	374105	
		9/22/2019							
E11	F16	9/18/2014	-	-	-		Yes	337284	
E12	F24	8/5/2013	-	-	-		No	140630[a]	
		8/10/2013						141112[a]	
E13	F24	6/6/2015	-	-	-		No	136355[a]	
		6/12/2015						150717[a]	
E14	F24	6/3/2016–9/15/2016	-	-	-		No	350704	

[a]Anticyclonic eddy.

of 15 μmol kg^{-1} are generally flat throughout the year, but are uplifted on density surfaces for weeks or months around the events manifest at 100 m. The uplift of the iso-nitrate surface of 15 μmol kg^{-1} is particularly well-defined for E1, E4, E5, and E6.

Six of the 14 of the events where nitrate >1 μmol kg^{-1} at 100 m depth were not associated with nitrate perturbations deeper in the water column (Figure 7). While three of these events (E12–E14) occur with nitrate >15 μmol kg^{-1} at 300 m, these all occur in F24, which occurs near the boundary of the gyre where the nitracline is shallower (Figure 4). Nitrate sections plotted against density for these events (Figure 8), indicate that there is not an isopycnal increase of nitrate near 300 m for any of these six events. Additionally, only two of these six events, E10 and E11, show evidence of nitrate increasing isopycnally at 100 m depth.

Next the events are examined for their location within the local eddy field, and their possible connection to the development of surface blooms of chl. The injection events are examined first (E1–E8, Figure 9), and then the events without diapycnal mixing (E9–E14, Figure 10).

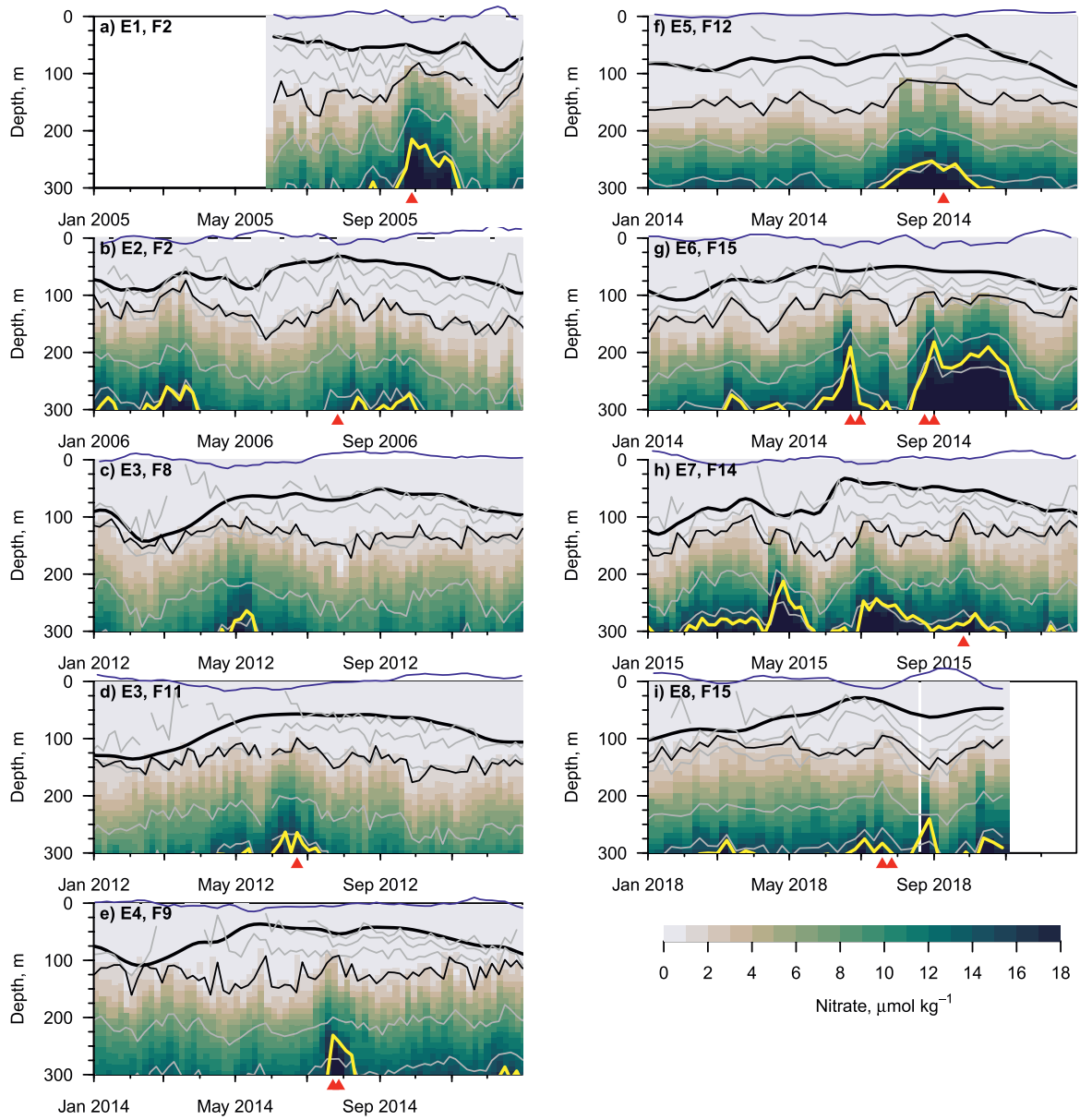

Figure 5. Nitrate versus depth (0–300 m) sections for the eight injection events when the nitracline reached 100 m during the summer, coincident with a nitrate increase at 300 m. The red triangles along the time axes indicate when nitrate >1.0 µmol kg^{-1} at 100 m depth during spring and summer (June–September). The black triangles indicate when nitrate >1.0 µmol kg^{-1} at 100 m depth during the rest of the year. E3 was observed by both F8 (c) and F11 (d). For consistency the *x*-axis for all sections covers one year, however the year differs for the different floats. The mixed-layer depth is indicated by the thick black line, isopycnal contours are shown in gray, and the nitrate isoclines of 1 and 15 µmol kg^{-1} are shown by black and yellow lines respectively. The sea-level anomalies (SLA) anomaly is indicated by the blue line. The SLA (in units of m) was multiplied by −100 to fit on the *y*-axis scale of the plots.

The first event, E1, occurred just south of Kauai in September–October 2005. Nitrate was elevated at 300 m between September–November (Table 2). When the injection first started in early September, the float was within an area of positive SLA, although the feature was not classified as an eddy. This feature was due north of cyclonic eddy 274078 (Figure 9a). At the end of the month, when the injection reached 100 m, a portion of cyclonic eddy 274078 was being pinched off and moved into the location of the float (Figure 9b). In early October this feature detached and became eddy 275928 (Figure 9c). At the end of September there was a small increase in surface chl (<0.1 mg m^{-3}) within the area of the newly forming cyclonic eddy. A month later, at the end of October, surface chl values near 0.1 mg m^{-3} were present within the just formed

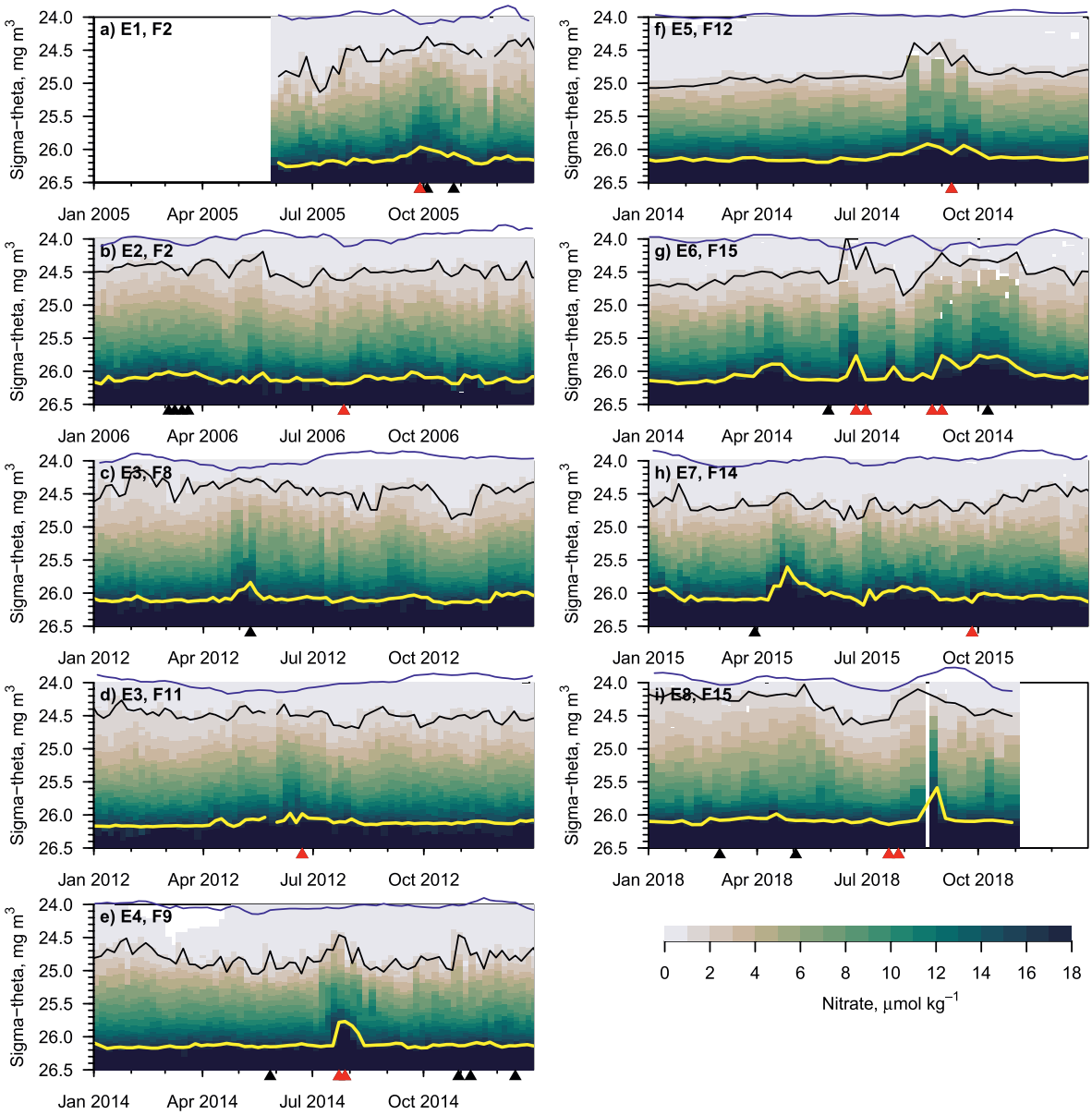

Figure 6. Nitrate versus sigma-theta (24–26.5 kg m^{-3}) sections for the eight injection events when the nitracline reached 100 m during the summer, coincident with a nitrate increase at 300 m. The red triangles along the time axes indicate when nitrate >1.0 µmol kg^{-1} at 100 m depth during summer (June–September). The black triangles indicate when nitrate >1.0 µmol kg^{-1} at 100 m depth during the rest of the year. For consistency the *x*-axis for all sections covers one year, however the year differs for the different floats. The nitrate isoclines of 1 and 15 µmol kg^{-1} are shown by black and yellow lines respectively. The sea-level anomalies (SLA) anomaly is indicated by the blue line. The SLA (in units of m) was multiplied by −1 and offset by 24 to fit on the *y*-axis scale of the plots.

eddy 275928, and also within an anticyclonic eddy just south of it. The injection lasted 62 days, during which the float drifted 24 km.

The second event, E2, developed in July–September 2006 in the frontal zone between cyclonic eddy 279677 and an anticyclonic eddy (Figure 9c). The nitracline shoaled above 100 m at the end of July, before the nitrate increase at 300 m between August 13 and September 26 (Table 2). Surface chl was already >0.1 mg m^{-3} in the northern part of the eddy portion when the nitrate injection started. Over the course of the injection, the cyclonic eddy moved north of the float and transformed into eddy 282281, a smaller and more circular feature than eddy 279677. For the latter part of the injection, the float moved counterclockwise around the periphery of eddy 282281. The injection lasted 44 days, during which the float drifted 141 km.

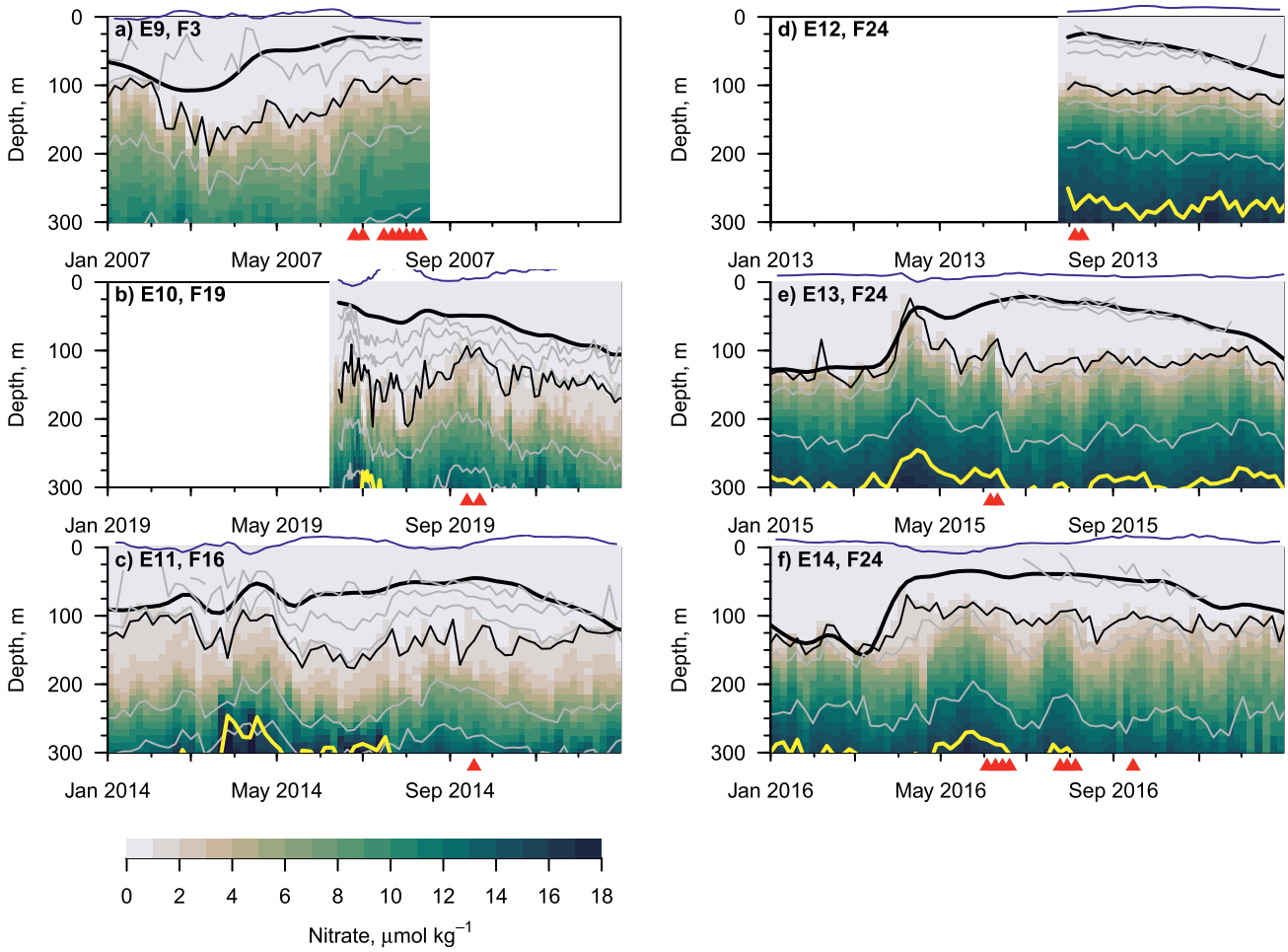

Figure 7. Nitrate versus depth (0–300 m) sections for the six events when the nitracline reached 100 m during the summer, without a nitrate increase at 300 m. The red triangles along the time axes indicate when nitrate >1.0 µmol kg^{-1} at 100 m depth during spring and summer (June–September). The black triangles indicate when nitrate >1.0 µmol kg^{-1} at 100 m depth during the rest of the year. E3 was observed by both F8 (c) and F11 (d). For consistency the *x*-axis for all sections covers one year, however the year differs for the different floats. The mixed-layer depth is indicated by the thick black line, isopycnal contours are shown in gray, and the nitrate isoclines of 1 and 15 µmol kg^{-1} are shown by black and yellow lines respectively. The sea-level anomalies (SLA) anomaly is indicated by the blue line. The SLA (in units of m) was multiplied by −100 to fit on the *y*-axis scale of the plots.

The third event, E3, occurred May–July of 2012, and was observed by both F8 and F11. The event had two injections, one in May that is observed in both F8 (Figure 5c) and F11 (Figure 5d), and one in June that was just observed in F11. At the start of the May injection both floats were near the center of cyclonic eddy 337839. The two floats had different trajectories with respect to the eddy. F8 traveled counterclockwise around the periphery of it, while F11 traveled westward, staying within the eddy as it also moved westward. Over the course of the two injections, the eddy moved westward and transformed into eddy 323099. The eddy moved faster than F11, so that at the start of the May injection F11 was on the west side of the eddy, and at the end of the second injection it was on the east side of the eddy. At the start of the second injection, in the beginning of June, F11 had moved closer to the eddy center, whereas F8 had moved further from it, which would explain why F8 did not observe an injection event in June. The first injection (as seen in F8) injection lasted 10 days and spanned a distance of 47 km, and the two F11 injections lasted 57 days and spanned a distance of 142 km (Table 2). Elevated chl developed (Figure 9h) in a filament encircling the southeast periphery of the eddy in early June. The areas of higher chl around 23.5°N are over seamounts in the Hawaiian-Emperor seamount chain where chl is always higher (Figure 1).

The fourth event, E4, occurred in July–August of 2014 along the edge of cyclonic eddy 337839 (Figure 10a). The nitracline shoaled above 100 m in early September, about 6 weeks after the nitrate increase at 300 m

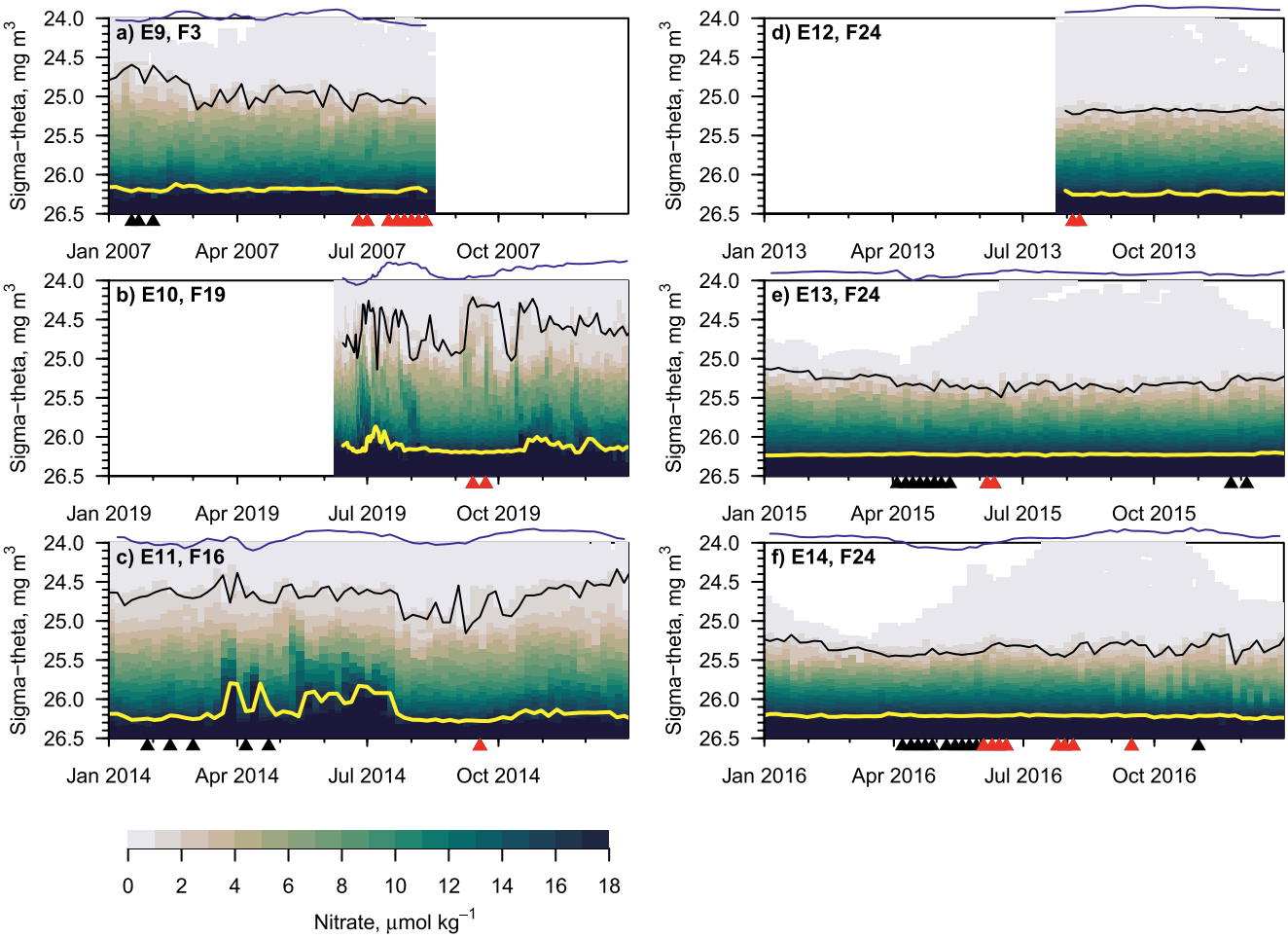

Figure 8. Nitrate versus sigma-theta (24–26.5 kg m^{-3}) sections for the six events when the nitracline reached 100 m during the summer, without a nitrate increase at 300 m. The red triangles along the time axes indicate when nitrate >1.0 µmol kg^{-1} at 100 m depth during summer (June–September). The black triangles indicate when nitrate >1.0 µmol kg^{-1} at 100 m depth during the rest of the year. For consistency the *x*-axis for all sections covers one year, however the year differs for the different floats. The nitrate isoclines of 1 and 15 µmol kg^{-1} are shown by black and yellow lines respectively. The sea-level anomalies (SLA) anomaly is indicated by the blue line. The SLA (in units of m) was multiplied by −1 and offset by 24 to fit on the *y*-axis scale of the plots.

(Table 2). Surface chl >0.1 mg m^{-3} was present at the start of the injection event. It was distributed predominately in a region of positive SLA just north of the cyclonic eddy, although this region was not identified as an anticyclonic eddy. The injection lasted 16 days, during which the float drifted 30 km.

The fifth event, E5, occurred in July–October of 2014 along the edge of cyclonic eddy 335139 (Figure 10d). The nitracline shoaled above 100 m at the end of July, at the same time as the nitrate increase at 300 m (Table 2). During the injection the eddy moved northwest, past F12, so that at beginning of the injection the float was on the west side of the eddy, and at the end of the injection it was on the east side of the eddy. Elevated chl developed along the periphery of the eddy at the end of August and as the bloom further developed it almost completely wrapped around the cyclonic eddy (Figure 10f). The injection lasted 92 days, during which the float drifted 76 km (Table 2). Two other floats, F10 and F13, were slightly north of the eddy at this time, but no injection events occurred in their data (Figure S1 in Supporting Information S1). It is interesting to note that while E5 was one of the stronger events in terms of isopycnal nitrate increases, it was associated with the weakest eddy, in terms of not having much of a signature in the SLA field (Figures 6f and 10d–10f).

The sixth event, E6 consisted of two injections, one occurring in May–June 2014, and another in August–November 2014. The August injection developed along the northwest periphery of cyclonic eddy 335073

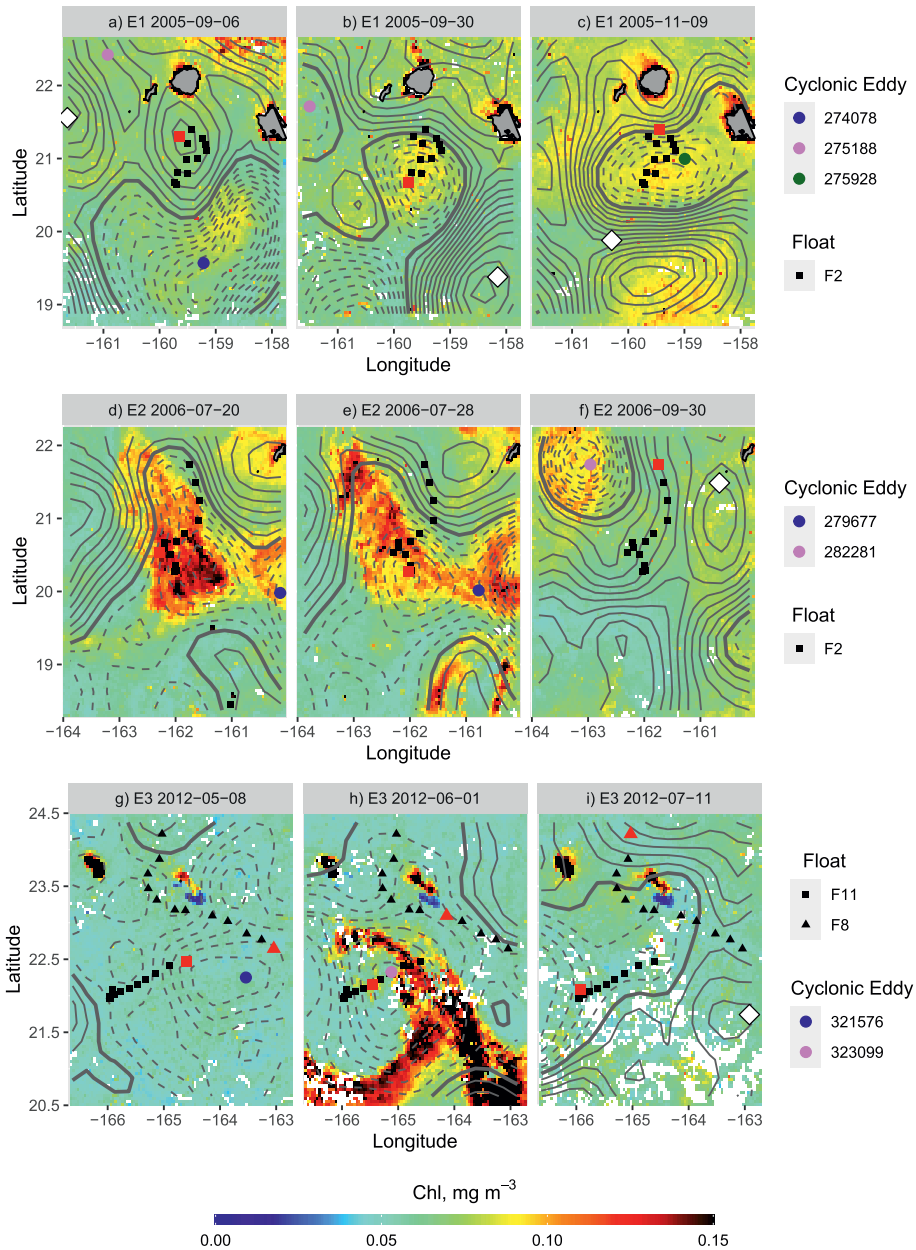

Figure 9. Float locations during injection events E1 (a–c), E2 (d–f) and E3 (g–i) overlain on maps of surface chl and sea-level anomalies (SLA) contours. Positions of cyclonic eddies are indicated by colored circles and anticyclonic eddies are shown as white triangles. The data on the first maps shown for each event correspond to the beginning of the nitrate injection as determined by the nitrate concentration at 300 m. The middle maps show data at the time of the nitrate anomaly at 100 m. The third maps show data at the end of the injection, or at the end of the maximum chl bloom development. Float locations for the entire period of the injection are shown in black. The most synoptic float location is shown in red. Contours of SLA are shown in gray. Negative SLA are shown as dashed lines, positive SLA are solid lines, and the zero SLA contour lines are thicker. For consistency all maps span four degrees of longitude and latitude.

(Figure 10g). The eddy moved northwest toward the float location, and at the end of the injection the float was just outside the southeast periphery of the eddy. Elevated chl developed within the interior of the eddy at the same time as the injection started. The injection lasted 93 days, during which the float drifted 216 km (Table 2).

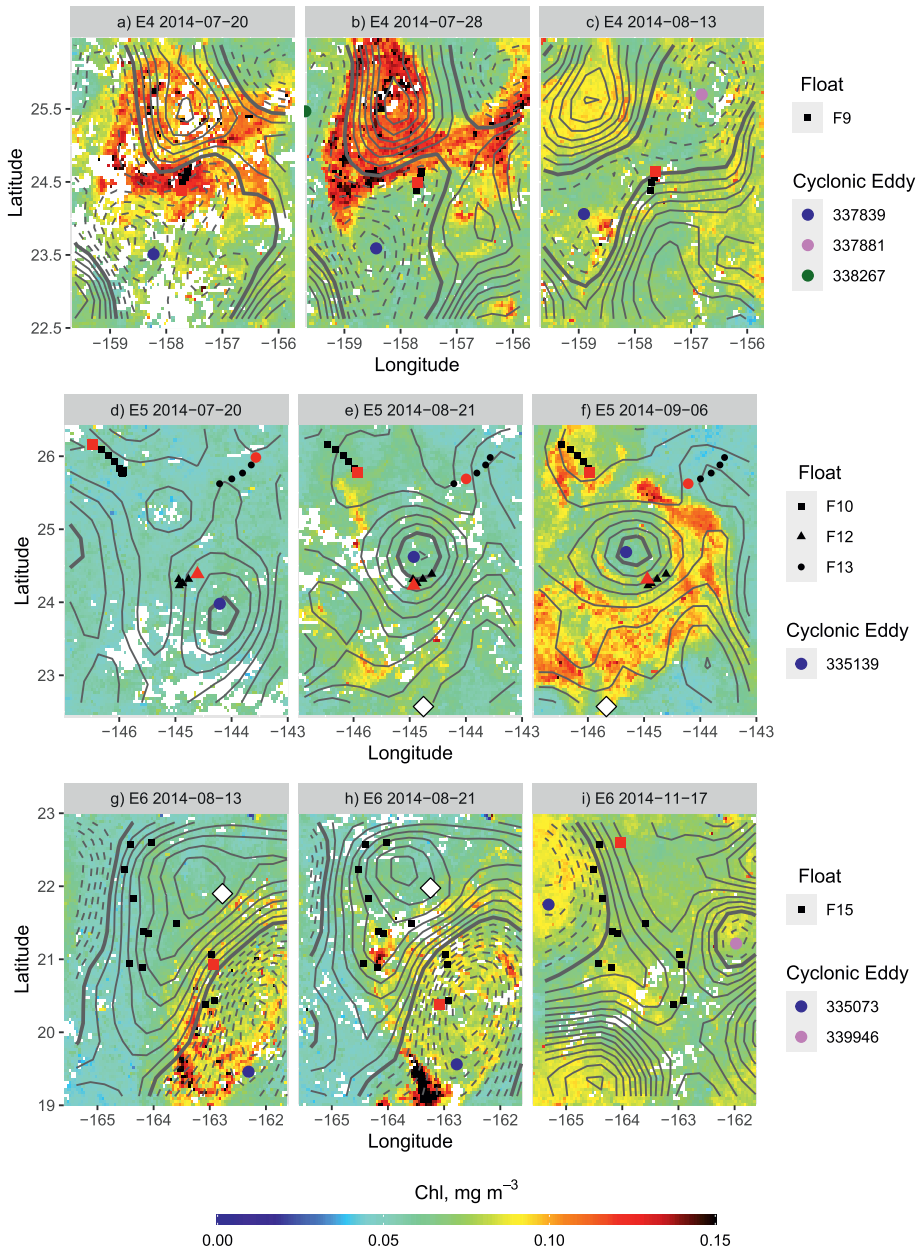

Figure 10. Float locations during injection events E4 (a–c), E5 (d–f) and E6 (g–i) overlain on maps of surface chl and sea-level anomalies (SLA) contours. Positions of cyclonic eddies are indicated by colored circles and anticyclonic eddies are shown as white triangles. The data on the first maps shown for each event correspond to the beginning of the nitrate injection as determined by the nitrate concentration at 300 m. The middle maps show data at the time of the nitrate anomaly at 100 m. The third maps show data at the end of the injection, or at the end of the maximum chl bloom development. Float locations for the entire period of the injection are shown in black. The most synoptic float location is shown in red. Contours of SLA are shown in gray. Negative SLA are shown as dashed lines, positive SLA are solid lines, and the zero SLA contour lines are thicker. For consistency all maps span four degrees of longitude and latitude.

The seventh event, E7, occurred July–October 2015. It initiated along the periphery of cyclonic eddy 342578 (Figures 11a), which merged with cyclonic eddy 344355 on July 4 to form cyclonic eddy 345123 (Figures 11b). The subsurface injection started July 3. Elevated first developed in late July within the interior of the cyclonic eddy (Figure 11b), and in early August a streak of higher chl developed outside of the cyclonic eddy, in the area where the injection was first observed (Figures 11c). The nitracline shoaled above 100 m

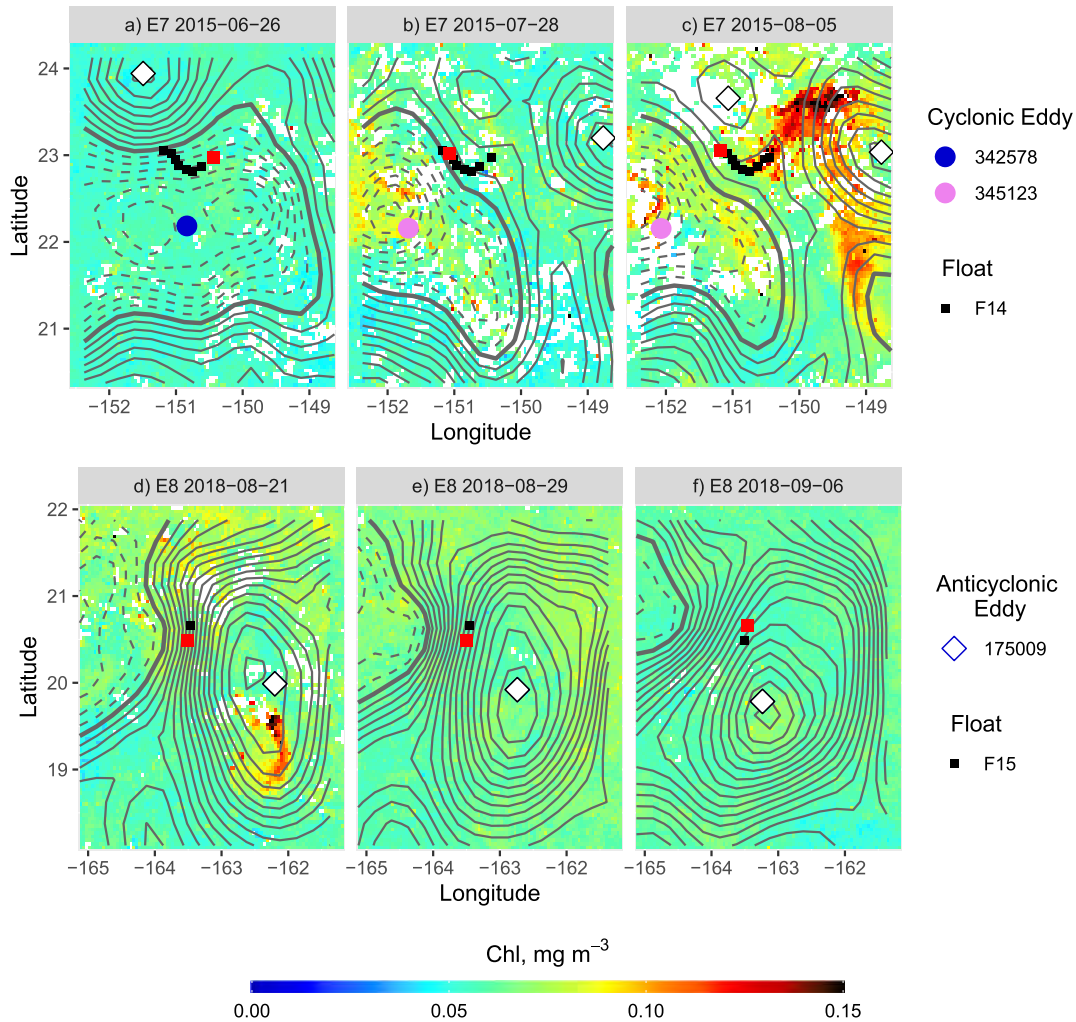

Figure 11. Float locations during injection events E7 (a–c) and E8 (d–f) overlain on maps of surface chl and sea-level anomalies (SLA) contours. Positions of cyclonic eddies are indicated by colored circles and anticyclonic eddies are shown as white triangles. The data on the first maps shown for each event correspond to the beginning of the nitrate injection as determined by the nitrate concentration at 300 m. The middle maps show data at the time of the nitrate anomaly at 100 m. The third maps show data at the end of the injection, or at the end of the maximum chl bloom development. Float locations for the entire period of the injection are shown in black. The most synoptic float location is shown in red. Contours of SLA are shown in gray. Negative SLA are shown as dashed lines, positive SLA are solid lines, and the zero SLA contour lines are thicker. For consistency all maps span four degrees of longitude and latitude.

at the end of September, about 12 weeks after the nitrate increase at 300 m (Table 2). The injection lasted 111 days, during which the float drifted 295 km (Table 2).

The eighth event, E8, occurred June–August 2018 (Figures 11d). The nitracline shoaled up to 100 m in mid-July (Figure 5i) during the passing of a cyclonic eddy (data not shown). At the end of August there was a sharp shoaling of the nitrate = 15 μmol kg^{-1} isocline that lasted for just one profile. This injection event occurred in the periphery of an anticyclonic eddy (Figures 11d). Some higher chl was present in the center of the anticyclonic eddy a week prior to the injection, but it did not develop further. This is the only mixing event that occurred within an anticyclonic eddy.

Next the events without isopycnal mixing are examined. The first of these events, E9, occurred at the western periphery of cyclonic eddy 288000 (Figure 12a). The nitracline remained above 100 m between the end of June to the beginning on August 2007. During the time the cyclonic eddy moved westward and the end

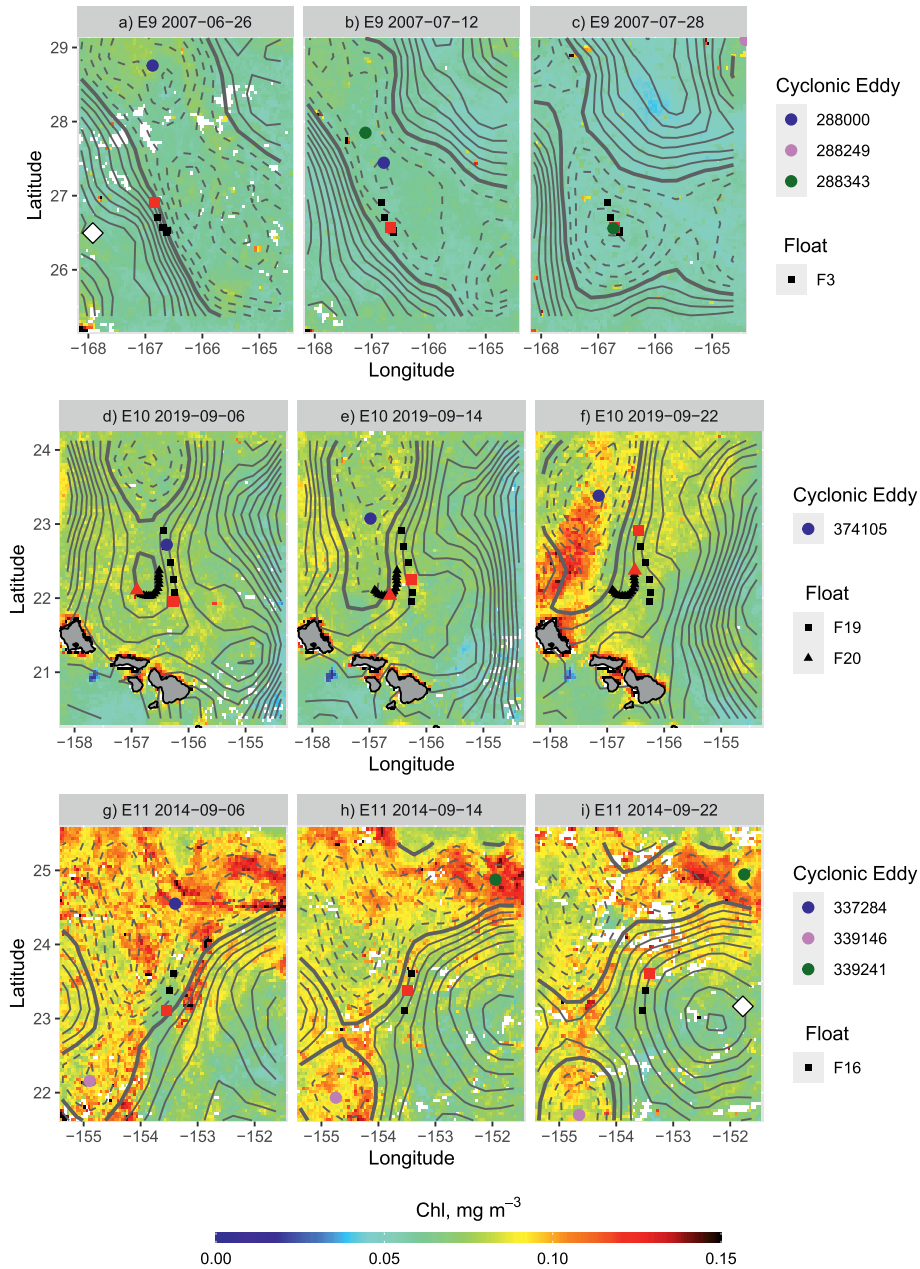

Figure 12. Float locations during events E9 (a–c), E10 (d–f), and E11 (g–i) overlain on maps of surface chl and sea-level anomalies (SLA) contours. Positions of cyclonic eddies are indicated by colored circles and anti-cyclonic eddies are shown as white triangles. The data on the first maps shown for each event correspond to the beginning of the nitrate injection as determined by the nitrate concentration at 300 m (Table 2). The middle maps show data at the time of the nitrate anomaly at 100 m, The third maps show a later time to best indicate the development of a surface chl bloom. Float locations for the entire period of the injection are shown in black. The most synoptic float location is shown in red. Contours of SLA are shown in gray. Negative SLA are shown as dashed lines, positive SLA are solid lines, and the zero SLA contour lines are thicker. For consistency all maps span four degrees of longitude and latitude.

of the injection it was in the center of the eddy. The quality adjusted data for this float stopped during the event (Figure 7a). There was no sign of elevated surface chl associated with this event (Figures 12a–12c).

Event E10 occurred at the southern periphery of cyclonic eddy 374105 in early September 2019 (Figure 12d). There were two floats in this region, F19 and F20, but only F19 observed the nitracline shoaling above 100 m (Figures 7b and S1t in Supporting Information S1). While the nitracline was above 100 m, elevated chl

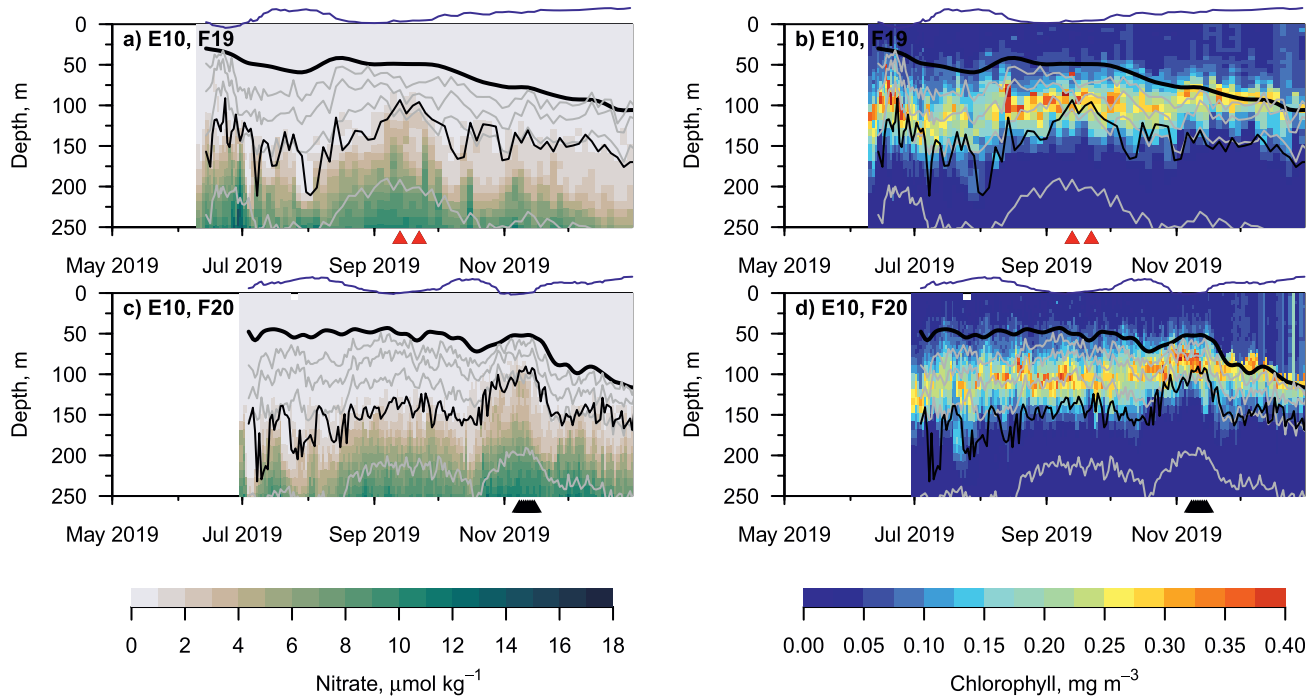

Figure 13. Surface (0–250 m) nitrate and chl sections for F19 (a and b) and F20 (c and d) during E10. The red and black triangles along the time axes indicate when nitrate >1.0 µmol kg^{-1} at 100 m depth during summer (red) and the rest of the year (black). The mixed-layer depth is indicated by the thick black line, isopycnal contours are shown in gray, and the nitrate isoclines of 1 µmol kg^{-1} are shown by black lines. The sea-level anomalies (SLA) anomaly is indicated by the blue line. The SLA (in units of m) was multiplied by −80 to fit on the *y*-axis scale of the plots.

developed in the center of the cyclonic eddy, but not in the location of the float. E10 was the only event that was observed by a float with a chl sensor on it (F19, Table 1). There was also another float (F20) near F19 during this event (Figures 12d–12f). Both F19 and F20 show a slight increase in the deep chl maximum associated with the shoaling nitracline (Figure 13). At the beginning of August the nitracline observed by F19 shoaled from deeper than 200 to ~125 m depth, after which chl values in the deep chl maximum increased to >0.3 mg m^{-3}.

Event E11 at the southern periphery of cyclonic eddy 337284 in early September 2014 (Figure 12g). There was elevated chl present throughout the cyclonic eddy.

Event E12 occurred at the boundary between two anticyclonic eddies in November 2014 (Figure 14a). There was a small patch of chl >0.1 mg m^{-3} already present to the west of the float when the nitracline shoaled above 100 m.

Event E13 occurred at the boundary between two anticyclonic eddies in April–June 2015 (Figure 14d). There was no sign of elevated surface chl associated with this event.

Event E14 started in the center of cyclonic eddy 350704 in May 2015 (Figure 14g). There was no sign of elevated surface chl associated with this event.

It appears that cyclonic eddies are more important than anticyclonic eddies for nutrient injections in the NPSG, which is not surprising since eddy pumping in the center of cyclonic eddies lifts isopycnals and the nitracline (McGillicuddy, 2016). Seven of the eight injection events occurred within cyclonic eddies, the other event (E8) occurred in the periphery of an anticyclonic eddy. Eddy-eddy interactions can lead to frontogenesis and strong vertical velocities at eddy peripheries (Lévy, 2008; Mahadevan et al., 2008; Spall & Richards, 2000), and this process has been attributed to the formation of blooms in the NPSG (Calil et al., 2011; Calil & Richards, 2010; Guidi et al., 2012). Which raises the question of whether the observed diapycnal mixing occurs primarily at the eddy periphery or the eddy center?

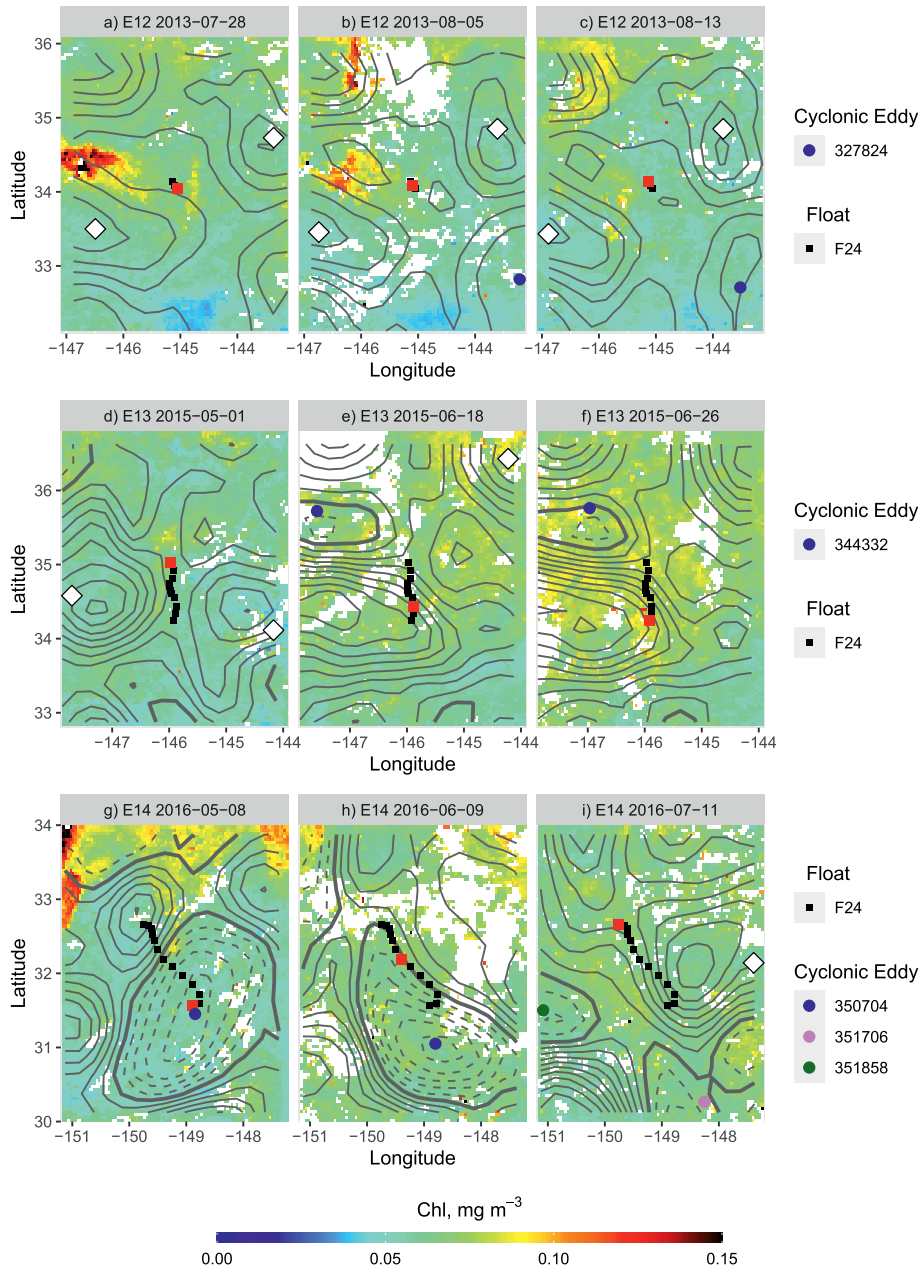

Figure 14. Float locations during events E12 (a–c), E13 (d–f), and E14 (g–i) overlain on maps of surface chl and sea-level anomalies (SLA) contours. Positions of cyclonic eddies are indicated by colored circles and anti-cyclonic eddies are shown as white triangles. The data on the first maps shown for each event correspond to the beginning of the nitrate injection as determined by the nitrate concentration at 300 m (Table 2). The middle maps show data at the time of the nitrate anomaly at 100 m, The third maps show a later time to best indicate the development of a surface chl bloom. Float locations for the entire period of the injection are shown in black. The most synoptic float location is shown in red. Contours of SLA are shown in gray. Negative SLA are shown as dashed lines, positive SLA are solid lines, and the zero SLA contour lines are thicker. For consistency all maps span four degrees of longitude and latitude.

Due to the transitory nature of both the floats and the eddies it can be difficult to follow where the floats are in relation to the eddy field. For three (E1, E3, and E7) of the eight injection events the isopycnal mixing appears concentrated within the center of the cyclonic eddy, as the nitrate isoclines are elevated coincident with the local minimum in SLA values (the blue lines on Figures 4 and 5). However, the local SLA minimum of the float trajectory does not necessarily correspond to the center of eddy. From examining the eddy

and the float trajectories (Figures 9–11) it can been seen that three of the mixing events occurred when the eddy passed over the float (E3, E5, E6) and the injection occurred in both the periphery and the center of the eddy. Two of the mixing events (E1 and E2) occurred as a new eddy was being shed off of an existing eddy and mixing was observed in both the periphery and the center of the eddy. The other three events (E4, E7, and E8) were confined to the periphery of the eddy, however none of these floats entered into the center of the eddies so it is possible the injection did in fact extend into the center of the eddy, but just was not observed by the float.

Satellite chl data provide a nice complement to the float data, as they provide a more complete spatial picture of the result of these nutrient injections in the ocean surface. Five of the events (E1, E2, E3, E6, and E7) had elevated chl develop within the center of the cyclonic eddy after the injection, consistent with the eddy pumping mechanism. One of the events (E4) had elevated chl develop in the frontal zone between the cyclonic eddy and an anticyclonic feature (Figures 10a and 10b), and the bloom intensified within the anticyclonic feature. In a similar fashion, in E5 elevated chl developed in the convergent zone around the outside of the cyclonic eddy (Figure 10f). These chl patterns are consistent with those described previously in this area, where the chl is distributed by horizontal stirring (Calil et al., 2011; Calil & Richards, 2010; Guidi et al., 2012). E8 was the only event that occurred within an anticyclonic eddy. There was a small patch of elevated chl within the center of the anticyclonic eddy at the time of the injection (Figures 11d).

Just as the patchy distribution of the float profiles makes it impossible to determine the spatial extent of these mixing events, it also is not possible to determine the exact timing of the events. The start of an event as seen in the float observations does not necessarily indicate the actual start, since the float could have just moved into an area where mixing was already occurring. Evidence for this is given by satellite observations of elevated chl in the vicinity of floats coincident with the "start" of an injection event (E2, E4, E6, and E8).

Of the six events where the nitracline shoaled without isopycnal mixing, four occurred within cyclonic eddies, and two occurred between two anticyclonic eddies (E12 and E13). Eddies are ubiquitous in the oceans and most of the float profiles occur near an eddy. There is a roughly equally likelihood of a float profile being close to a cyclonic eddy, an anticyclonic eddy, or no eddy (Table 4). Profiles with nitrate >15 μmol kg^{-1} at 300 m, used here as an indication of potential diapycnal mixing, had a greater likelihood of being close to a cyclonic eddy relative to all profiles (46% vs. 35%). But clearly cyclonic eddies do not always generate nutrient injections, because they happen much less frequently than the amount of time that floats are within cyclonic eddies.

Eddy age has been proposed to play a role in the biogeochemical properties of mesoscale eddies (Sweeney et al., 2003), with nutrients being upwelled into the euphotic zone during eddy initiation. To determine when the injection events occurred within the eddy evolution, the rotational eddy speed is shown over the duration of the eddies associated with each mixing event (Figure 15). There is no consistent relationship between when the injections occur (the yellow boxes on Figure 15) and the eddy age (Table 2). While the E7 injection occurred at the initiation of a new eddy from the merging of two eddies (Figure 15g), the other events occurred when the eddy was between 0.8–6 months old.

However, many of the injection events occurred coincident with a change in eddy dynamics (Table 3). E1 and E2 occurred at the periphery of an eddy being shed off an existing eddy (Figures 9a–9f) and the E4 and E7 injections occurred during the merging of two eddies. Four of the nine (counting two as part of E3) injections develop during a change in eddy speed. Both of the injections that were part of E3, started at a maximum of eddy speed, when the eddy motion changed from increasing in speed to decreasing (Figures 14c and 14h). The E4 and E6 injections started coincident with an increase in eddy speed (Figures 14d and 14f). The initiation of some of these mixing events being coincident with a change in eddy speed confirms the hypothesis put forth by Nencioli et al. (2008) that translation speed is a fundamental factor in determining the biogeochemical characteristics of a cyclonic eddy. They proposed that rather than nutrient injection being limited to a single event when the eddy is initially spun-up, it can occur continuously, through a horizontal leaky exchange that occurs as the eddy moves. The observations seen here provide evidence that a change in the rotational eddy speed can bring about nutrient injection.

Six of the mixing events started in the periphery of a cyclonic eddy which was flanked by an anticyclonic eddy, with a strong frontal zone between the two eddies (Table 3). Modeling studies have suggested that

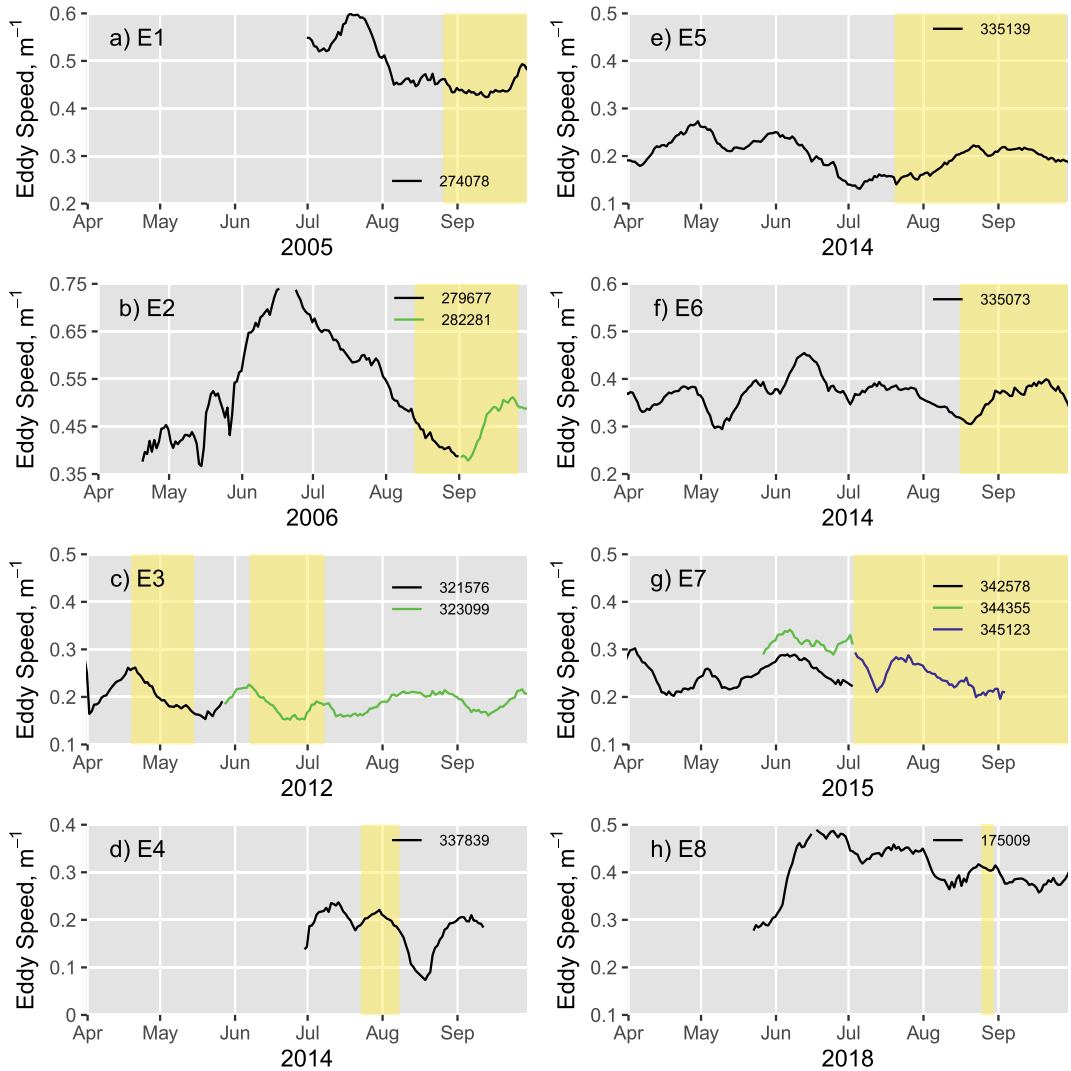

Figure 15. Timeseries of the speed of the eddies in which a subsurface injection was observed for E1 (a), E2 (b), E3 (c), E4 (d), E5 (f), E6 (g), E7 (g) and E8 (h). The yellow boxes indicate the timing of the subsurface injection events. The ranges of the eddy speed *y*-axes vary, but for consistency they always span 0.4 m sec^{-1}.

Table 3
Summary of the Locations Within the Eddy for the Eight Injection Events, and Any Eddy Dynamics Associated With the Injection Event

Event	Eddy location	Eddy dynamic
E1	Periphery & Center	Eddy shedding, frontal area
E2	Periphery & Center	Eddy shedding, frontal area
E3	Periphery & Center	Speed change
E4	Periphery	Eddy merging, frontal area, speed change
E5	Periphery & Center	
E6	Periphery & Center	Frontal area, speed change
E7	Periphery	Eddy merging, frontal area, speed change
E8	Periphery	Anticyclonic Eddy, frontal area

large vertical velocities could develop in submesoscale frontal zones as the result of ageostrophic secondary circulation (Lapeyre & Klein, 2006; Lévy, 2008; Mahadevan & Tandon, 2006). However, there has been debate about how relevant this process is (Mahadevan et al., 2008; McGillicuddy et al., 2008), particularly in the NPSG (Ascani et al., 2013). The observation that six of the eight mixing events observed by the BGC-Argo floats initiated in the frontal zone between eddies provides evidence that the frontal zone plays an important role in vertical advection of nutrients in the NPSG.

E5 is the only mixing event that does not develop coincident with a change in eddy dynamics or within a frontal zone between two eddies. While this event had pronounced isopycnal mixing at the nitracline, it occurred within the weakest eddy of all of the eight events, as seen by the little variation in SLA along the float trajectory (Figure 6f), and also within the larger area around the float and eddy (Figures 10d–10f). This

Table 4
Percentage of Float Profiles That Were Near a Cyclonic Eddy, an Anticyclonic Eddy, or Were Not Near an Eddy

	N	Cyclonic eddy	Anticyclonic eddy	No eddy
All profiles	5,130	35%	36%	29%
$N_{300m} > 15$	785	46%	28%	27%

Note. Percentages are shown for all floats (excluding F23 and F25), and for the subset of those floats with nitrate >15 μmol kg^{-1} at 300 m depth.

inconsistency suggests that there are additional dynamics involved with generating nitrate injections within eddies, and underscores the complexity of the impacts of eddies on ocean biogeochemistry.

These results build upon the previous studies that used BGC-Argo data to look at nutrient injections in this region. Johnson et al. (2010) described short-lived events, <10 days, whereas the subsurface injections described here last 4–12 weeks. They observed nitrate injections accompanied by uplifted isopycnals, but also noted that enhanced mixing drove nitrate across isopycnals. In contrast, Ascani et al. (2013) concluded that nitrate injections are primarily the result of uplift of isopyncal surfaces. As shown here, both types of nitrate injections occur in the NPSG, sometimes nitrate anomalies are caused by a shoaling of isospycnals (E9–E14), and sometimes they are indicative of mixing events that can last weeks, and span hundreds of kilometers. While both these previous studies used the same data used here, they analyzed earlier (prior to 2012), smaller subsets of the data, and the events described here were not in the datasets that they analyzed. Clearly the episodic injection events described here involve significant mixing across isopycnal surfaces of water with higher nutrient concentrations. These mixing events occur predominately in cyclonic eddies (7 out of 8) that are undergoing eddy transformation and/or have a well-developed frontal zone between a cyclonic eddy and an anticyclonic eddy.

4. Conclusions

The nitrate data from 25 BGC-Argo floats (5,569 profiles) examined here showed 14 summer episodes of nitracline shoaling, when nitrate >1 μmol/kg at 100 m depth. While the perturbations at 100 m depth are often just seen in one profile, many of the events are part of a larger mixing event that extended down to 300 m depth. These events last 4–12 weeks, and span distances between 30–300 km, making them significantly larger events that have been previously reported for this region. Seven of the eight mixing events occurred in cyclonic eddies, and were followed by the development of a surface bloom of chl evident in the satellite data. The initiation of these events appears to be caused by changes in eddy dynamics, eddy speed or eddy transformation, and often in the frontal area between a cyclonic eddy and an anticyclonic eddy. The BGC-Argo data provide the first in situ data showing that the summer chl blooms in this region are driven by subsurface nutrient injections. These events are not obvious from just temperature and salinity data, which points to the importance of establishing a global array of BGC-Argo floats to better understand biophysical processes in the oceans.

Data Availability Statement

The BGC-Argo float data were obtained from https://biogeochemical-argo.org/data-access.php. These data were collected and made freely available by the International Argo Program and the national programs that contribute to it (https://argo.ucsd.edu, https://www.ocean-ops.org). The Argo Program is part of the Global Ocean Observing System (Argo, 2000). The OC-CCI (v5.0) chl satellite data were obtained from the ERDDAP maintained jointly by the SWFSC's Environmental Research Division and the West Coast regional node of NOAA's CoastWatch program at https://coastwatch.pfeg.noaa.gov/erddap/griddap/pmlEsaCCI50OceanColor8Day.html. The sea level anomaly data were produced by the Copernicus Climate Change Monitoring Services and are distributed at https://cds.climate.copernicus.eu/cdsapp#!/dataset/satellite-sea-level-global?tab=overview. The Mesoscale Eddy Trajectory Atlas products (Delayed Time Version 2.0) were produced by SSALTO/DUACS and distributed by AVISO+ at https://www.aviso.altimetry.fr/en/data/products/value-added-products/global-mesoscale-eddy-trajectory-product.html with support from CNES. They were developed and validated in collaboration with D. Chelton and M. Schlax at the Oregon State University.

Acknowledgments
Profiling float deployments were supported by NSF Grant 0825348, NOPP/Office of Naval Research Grant N00014-09-10052, and NOAA Grant NA17RJ1232. Processing and curation of data was supported by the Southern Ocean Carbon and Climate Observations and Modeling (SOCCOM) Project funded by National Science Foundation, Division of Polar Programs (NSF PLR-1425989). The float data were collected and made freely available by the International Argo Program and the national programs that contribute to it (https://argo.ucsd.edu, https://www.ocean-ops.org). The Argo Program is part of the Global Ocean Observing System. Thanks to NOAA's CoastWatch program (West Coast Node) for making satellite data available on ERDDAP. Reviews by four anonymous reviewers improved this manuscript.

References

Anderson, E. E., Wilson, C., Knap, A. H., & Villareal, T. A. (2018). Summer diatom blooms in the easterm North Pacific gyre investigated with a long-endurance autonomous surface vehicle. *PeerJ*, *6*, e5387. https://doi.org/10.7717/peerj.5387

Argo. (2000). *Argo float data and metadata from Global Data Assembly Centre (Argo GDAC)*. https://doi.org/10.17882/42182

Ascani, F., Richards, K. J., Firing, E., Grant, S., Johnson, K. S., Jia, Y., et al. (2013). Physical and biological controls of nitrate concentrations in the upper subtropical North Pacific Ocean. *Deep Sea Research Part II: Topical Studies in Oceanography*, *93*, 119–134. https://doi.org/10.1016/j.dsr2.2013.01.034

Benitez-Nelson, C. R., & McGillicuddy, D. J., Jr. (2008). Mesoscale physical-biological-biogeochemical linkages in the open ocean: An introduction to the results of the E-Flux and EDDIES programs. *Deep-Sea Research, II*, *55*, 1133–1138. https://doi.org/10.1016/j.dsr2.2008.03.001

Bittig, H. C., Maurer, T. L., Plant, J. N., Schmechtig, C., Wong, A. P. S., Claustre, H., et al. (2019). A BGC-argo guide: Planning, deployment, data handling and usage. *Frontiers in Marine Science*, *6*. https://doi.org/10.3389/fmars.2019.00502

Bittig, H. C., Steinhoff, T., Claustre, H., Fiedler, B., Williams, N. L., Sauzède, R., et al. (2018). An alternative to static climatologies: Robust estimation of open ocean CO_2 variables and nutrient concentrations from T, S, and O_2 data using Bayesian neural networks. *Frontiers in Marine Science*, *5*(328). https://doi.org/10.3389/fmars.2018.00328

Bittig, H. C., Wong, A., & Plant, J., & the Coriolis Argo data management team. (2021). *BGC-Argo synthetic profile file processing and format on Coriolis GDAC, V1.21*. https://doi.org/10.13155/55637

Calil, P. H. R., Doney, S. C., Yumimoto, K., Eguchi, K., & Takemura, T. (2011). Episodic upwelling and dust deposition as bloom triggers in low-nutrient, low-chlorophyll regions. *Journal of Geophysical Research*, *116*. https://doi.org/10.1029/2010JC006704

Calil, P. H. R., & Richards, K. J. (2010). Transient upwelling hot spots in the oligotrophic North Pacific. *Journal of Geophysical Research*, *115*. https://doi.org/10.1029/2009JC005360

Chelton, D. B., Schlax, M. G., & Samelson, R. M. (2011). Global observations of nonlinear mesoscale eddies. *Progress in Oceanography*, *91*, 167–216. https://doi.org/10.1016/j.pocean.2011.01.002

Claustre, H., Johnson, K. S., & Takeshita, Y. (2020). Observing the global ocean with biogeochemical-argo. *Annual Review of Marine Science*, *12*, 23–48. https://doi.org/10.1146/annurev-marine-010419-010956

Dong, J., Robertson, R., Dong, C., Hartlipp, P. S., Zhou, T., Shao, Z., et al. (2019). Impacts of mesoscale currents on the diurnal critical latitude dependence of internal tides: A numerical experiment based on Barcoo Seamount. *Journal of Geophysical Research*, *124*, 2452–2471. https://doi.org/10.1029/2018JC014413

Dore, J. E., Letelier, R. M., Church, M. J., & Karl, D. M. (2008). Summer phytoplankton blooms in the oligotrophic North Pacific subtropical gyre: Historical perspective and recent observations. *Progress in Oceanography*, *76*, 2–38. https://doi.org/10.1016/j.pocean.2007.10.002

Falkowski, P. G., Ziemann, D., Kolber, Z., & Bienfang, P. K. (1991). Role of eddy pumping in enhancing primary production in the ocean. *Nature*, *352*, 55–58. https://doi.org/10.1038/352055a0

Guidi, L., Calil, P. H. R., Duhamel, S., Bjoerkman, K. M., Doney, S. C., Jackson, G. A., et al. (2012). Does eddy-eddy interaction control surface phytoplankton distribution and carbon export in the North Pacific Subtropical Gyre? *Journal of Geophysical Research*, *117*. https://doi.org/10.1029/2012JG001984

Hibiya, T., Nagasawa, M., & Niwa, Y. (2007). Latitudinal dependence of diapycnal diffusivity in the thermocline observed using a microstructure profiler. *Geophysical Research Letters*, *34*, L24602. https://doi.org/10.1029/2007GL032323

Jayaram, C., Bhaskar, T. V. S. U., Kumar, J. P., & Swain, D. (2019). Cyclone enhanced chlorophyll in the Bay of Bengal as evidenced from satellite and BGC-argo float observations. *Journal of the Indian Society of Remote Sensing*, *47*, 1875–1882. https://doi.org/10.1007/s12524-019-01034-1

Johnson, K. S., Plant, J. N., Coletti, L. J., Jannasch, H. W., Sakamoto, C. M., Riser, S. C., et al. (2017). Biogeochemical sensor performance in the SOCCOM profiling float array. *Journal of Geophysical Research: Oceans*, *122*(8), 6416–6436. https://doi.org/10.1002/2017jc012838

Johnson, K. S., Riser, S. C., & Karl, D. M. (2010). Nitrate supply from deep to near-surface waters of the North Pacific subtropical gyre. *Nature*, *465*, 1062–1065. https://doi.org/10.1038/nature09170

Kara, A. B., Rochford, P. A., & Hurlburt, H. E. (2003). Mixed layer depth variability over the global ocean. *Journal of Geophysical Research*, *103*, 3079. https://doi.org/10.1029/2000JC000736

Karl, D. M., Bidigare, R. R., Church, M. J., Dore, J. E., Leteleir, R. M., Mahaffey, C., & Zehr, J. P. (2008). The nitrogen cycle in the North Pacific trades biome: An evolving paradigm. In D. G. Capone, D. A. Bronk, M. R. Mulholland, & E. J. Carpenter (Eds.), *Nitrogen in the marine environment* (pp. 705–769). Academic Press. https://doi.org/10.1016/b978-0-12-372522-6.00016-5

Karl, D. M., Church, M. J., Dore, J. E., Letelier, R. M., & Mahaffey, C. (2012). Predictable and efficient carbon sequestration in the North Pacific Ocean supported by symbiotic nitrogen fixation. *Proceedings of the National Academy of Sciences of the United States of America*, *109*, 1842–1849. https://doi.org/10.1073/pnas.1120312109

Karl, D. M., & Lukas, R. (1996). The Hawaii Ocean Time-series (HOT) program: Background, rationale and field implementation. *Deep-Sea Research, II*, *43*, 129–156. https://doi.org/10.1016/0967-0645(96)00005-7

Landry, M. R. (2002). Integrating classical and microbial food web concepts: Evolving views from the open-ocean tropical Pacific. *Hydrobiologia*, *480*, 29–39. https://doi.org/10.1023/a:1021272731737

Lapeyre, G., & Klein, P. (2006). Impact of the small-scale elongated filaments on the oceanic vertical pump. *Journal of Marine Research*, *64*, 835–851. https://doi.org/10.1357/002224006779698369

Lehahn, Y., Koren, I., Sharoni, S., d'Ovidio, F., Vardi, A., & Boss, E. (2017). Dispersion/dilution enhances phytoplankton blooms in low-nutrient waters. *Nature Communications*, *8*, 14868. https://doi.org/10.1038/ncomms14868

Lévy, M. (2008). The modulation of biological production by oceanic mesoscale turbulence. *Lecture Notes in Physics*, *744*, 219–261. https://doi.org/10.1007/978-3-540-75215-8_9

Lotliker, A. A., Baliarsingh, S. K., Trainer, V. L., Wells, M. L., Wilson, C., Udaya Bhaskar, T. V. S., et al. (2018). Characterization of oceanic Noctiluca blooms not associated with hypoxia in the Northeastern Arabian Sea. *Harmful Algae*, *74*, 46–57. https://doi.org/10.1016/j.hal.2018.03.008

MacKinnon, J. A., & Winters, K. B. (2005). Subtropical catastrophe: Significant loss of low-mode tidal energy at 28.9°. *Geophysical Research Letters*, *32*, https://doi.org/10.1029/2005GL023376

Mahadevan, A., & Tandon, A. (2006). An analysis of mechanisms for submesoscale vertical motion at ocean fronts. *Ocean Modeling*, *14*, 241–256. https://doi.org/10.1016/j.ocemod.2006.05.006

Mahadevan, A., Thomas, L. N., & Tandon, A. (2008). Comment on "Eddy/wind interactions stimulate extraordinary mid-ocean plankton blooms". *Science*, *320*, 448b. https://doi.org/10.1126/science.1152111

Martin, A. P., & Pondaven, P. (2003). On estimates for the vertical nitrate flux due to eddy pumping. *Journal of Geophysical Research*, *108*(C11), 3359. https://doi.org/10.1029/2003JC001841

Mayot, N., D'Ortenzio, F., Taillandier, V., Prieur, L., Fommervault, O. P. d., Claustre, H., et al. (2017). Physical and biogeochemical controls of the phytoplankton blooms in North Western Mediterranean Sea: A multiplatform approach over a complete Annual Cycle (2012–2013 DEWEX experiment). *Journal of Geophysical Research*, *122*, 9999–10019. https://doi.org/10.1002/2016jc012052

McGillicuddy, D. J., Jr. (2016). Mechanisms of physical-biological-biogeochemical interaction at the oceanic mesoscale. *Annual Review of Marine Science*, *8*, 125–159. https://doi.org/10.1146/annurev-marine-010814-015606

McGillicuddy, D. J., Jr., Ledwell, J. R., & Andersson, L. A. (2008). Response to comment on "Eddy/wind interactions stimulate extraordinary mid-ocean plankton blooms". *Science*, *320*, 448c. https://doi.org/10.1126/science.1148974

McGillicuddy, D. J., Jr., & Robinson, A. R. (1997). Eddy-induced nutrient supply and new production in the Sargasso Sea. *Deep-Sea Research*, *44*, 1427–1450. https://doi.org/10.1016/s0967-0637(97)00024-1

Nencioli, F., Kuwahara, V. S., Dickey, T. D., Rii, Y. M., & Bidigare, R. R. (2008). Physical dynamics and biological implications of a mesoscale eddy in the lee of Hawai'i: Cyclone Opal observations during E-Flux III. *Deep-Sea Research, II*, *55*, 1252–1274. https://doi.org/10.1016/j.dsr2.2008.02.003

Riser, S. C., & Johnson, K. S. (2008). Net production of oxygen in the subtropical ocean. *Nature*, *451*(7176), 323–325. https://doi.org/10.1038/nature06441

Sathyendranath, S., Brewin, R. J. W., Brockmann, C., Brotas, V., Calton, B., Chuprin, A., et al. (2019). An ocean-colour time series for use in climate studies: the experience of the Ocean-Colour Climate Change Initiative (OC-CCI). *Sensors*, *19*, 4285. https://doi.org/10.3390/s19194285

Sauzède, R., Claustre, H., Fommervault, O. P. d., Bittig, H. C., Gattuso, J.-P., Legendre, L., & Johnson, K. S. (2017). Estimates of water-column nutrients concentration and carbonate system parameters in the global ocean: A novel approach based on neural networks. *Frontiers in Marine Science*, *4*, 128. https://doi.org/10.3389/fmars.2017.00128

Sauzède, R., Martinez, E., Maes, C., Pasqueron de Fommervault, O., Poteau, A., Mignot, A., et al. (2020). Enhancement of phytoplankton biomass leeward of Tahiti as observed by Biogeochemical-Argo floats. *Journal of Marine Systems*, *204*, 103284. https://doi.org/10.1016/j.jmarsys.2019.103284

Schlax, M. G., & Chelton, D. B. (2016). *The "growing method" of eddy identification and tracking in two and three dimensions*. Retrieved from http://wombat.coas.oregonstate.edu/eddies/Growing_Method_of_Eddy_Identification_and_Tracking.pdf

Schmechtig, C., & Thierry, V., & the Bio Argo team. (2015). *Argo quality control manual for biogeochemical data*. https://doi.org/10.13155/40879

Seki, M. P., Polovina, J. J., Brainard, R. E., Bidigare, R. R., Leonard, C. L., & Foley, D. G. (2001). Biological enhancement at cyclonic eddies tracked with GOES thermal imagery in Hawaiian waters. *Geophysical Research Letters*, *28*, 1583–1586. https://doi.org/10.1029/2000gl012439

Shcherbina, A. Y., Gregg, M. C., Alford, M. H., & Harcourt, R. R. (2010). Three-dimensional structure and temporal evolution of submesoscale thermohaline intrusions in the North Pacific subtropical frontal zone. *Journal of Physical Oceanography*, *40*, 1669–1689. https://doi.org/10.1175/2010jpo4373.1

Simons, R. A. (2020). *ERDDAP, NOAA Southwest Fisheries Science Center*. NOAA/NMFS/SWFSC/ERD. Retrieved from http://coastwatch.pfeg.noaa.gov/erddap

Spall, S. A., & Richards, K. J. (2000). A numerical model of mesoscale frontal instabilities and plankton dynamics—I. Model formulation and initial experiments. *Deep Sea Research, I*, *47*, 1261–1301. https://doi.org/10.1016/s0967-0637(99)00081-3

Sweeney, E. N., McGillicuddy, D. J., Jr., & Buesseler, K. O. (2003). Biogeochemical impacts due to mesoscale eddy activity in the Sargasso Sea as measured at the Bermuda Atlantic Time-series Study (BATS). *Deep-Sea Research, II*, *50*, 3017–3039. https://doi.org/10.1016/j.dsr2.2003.07.008

Thierry, V., & Bittig, H. C., & the Argo-BGC team. (2021). *Argo quality control manual for dissolved oxygen concentration, V2.1*. https://doi.org/10.13155/46542

Villareal, T. A., Adornato, L. R., Wilson, C., & Schoenbaechler, C. A. (2011). Summer blooms of diatom-diazotroph assemblages and surface chlorophyll in the N. Pacific gyre—A disconnect. *Journal of Geophysical Research*, *116*. https://doi.org/10.1029/2010JC006268

Villareal, T. A., Brown, C. G., Brzezinski, M. A., Krause, J. W., & Wilson, C. (2012). Summer diatom blooms in the North Pacific Subtropical Gyre: 2008-2009. *PLoS One*, *7*, e33109. https://doi.org/10.1371/journal.pone.0033109

Villareal, T. A., Pilskaln, C., Brzezinski, M., Lipschultz, F., Dennet, M., & Gardner, G. B. (1999). Upward transport of oceanic nitrate by migrating diatom mats. *Nature*, *397*, 423–425. https://doi.org/10.1038/17103

Villareal, T. A., Pilskaln, C. H., Montoya, J. P., & Dennett, M. (2014). Upward nitrate transport by phytoplankton in oceanic waters: Balancing nutrient budgets in oligotrophic seas. *PeerJ*, *2*, e302. https://doi.org/10.7717/peerj.302

Ward, W. W., Kilpatrick, K. A., Renger, E. H., & Eppley, R. W. (1989). Biological nitrogen cycling in the nitracline. *Limnology & Oceanography*, *34*, 493–513. https://doi.org/10.4319/lo.1989.34.3.0493

White, A. E., Spitz, Y. H., & Letelier, R. M. (2007). What factors are driving summer phytoplankton blooms in the North Pacific Subtropical Gyre? *Journal of Geophysical Research*, *112*. https://doi.org/10.1029/2007JC004129

Wilson, C. (2011). Chlorophyll anomalies along the critical latitude at 30°N in the NE Pacific. *Geophysical Research Letters*, *38*. https://doi.org/10.1029/2011GL048210

Wilson, C., & Qiu, X. (2008). Global distribution of summer chlorophyll blooms in the oligotrophic gyres. *Progress in Oceanography*, *78*, 107–134. https://doi.org/10.1016/j.pocean.2008.05.002

Wilson, C., Villareal, T. A., Brzezinski, M. A., Krause, J. W., & Shcherbina, A. Y. (2013). Chlorophyll bloom development and the subtropical front in the North Pacific. *Journal of Geophysical Research*, *118*, 1473–1488. https://doi.org/10.1002/jgrc.20143

Xiu, P., & Chai, F. (2020). Eddies affect subsurface phytoplankton and oxygen distributions in the North Pacific Subtropical Gyre. *Geophysical Research Letters*, *47*, e2020GL087037. https://doi.org/10.1029/2020GL087037